Eur. Phys. J. C (2024) 84:27
https://doi.org/10.1140/epjc/s10052-023-12258-4

THE EUROPEAN PHYSICAL JOURNAL C

Regular Article - Experimental Physics

Measurement of the production cross section for a W boson in association with a charm quark in proton–proton collisions at $\sqrt{s} = 13$ TeV

CMS Collaboration*

CERN, 1211 Geneva 23, Switzerland

Received: 4 August 2023 / Accepted: 15 November 2023

Abstract The strange quark content of the proton is probed through the measurement of the production cross section for a W boson and a charm (c) quark in proton–proton collisions at a center-of-mass energy of 13 TeV. The analysis uses a data sample corresponding to a total integrated luminosity of 138 fb^{-1} collected with the CMS detector at the LHC. The W bosons are identified through their leptonic decays to an electron or a muon, and a neutrino. Charm jets are tagged using the presence of a muon or a secondary vertex inside the jet. The W + c production cross section and the cross section ratio $R_c^{\pm} = \sigma(W^+ + \bar{c})/\sigma(W^- + c)$ are measured inclusively and differentially as functions of the transverse momentum and the pseudorapidity of the lepton originating from the W boson decay. The precision of the measurements is improved with respect to previous studies, reaching 1% in $R_c^{\pm} = 0.950 \pm 0.005\,(\text{stat}) \pm 0.010\,(\text{syst})$. The measurements are compared with theoretical predictions up to next-to-next-to-leading order in perturbative quantum chromodynamics.

1 Introduction

The associated production of a W boson and a single charm (c) quark (W + c) in proton–proton (pp) collisions at the CERN LHC is directly sensitive to the strange quark (s) content of the colliding protons at an energy scale of the order of the W boson mass [1]. This sensitivity comes from the dominance of the sg $\rightarrow$ W + c contribution over the Cabibbo-suppressed process dg $\rightarrow$ W + c at tree level (see Fig. 1). Therefore, this process provides valuable information on the strange quark parton distribution function (PDF), which is one of the least constrained PDFs of the proton. Accurate measurements of the W + c production cross section and of the $R_c^{\pm} = \sigma(W^+ + \bar{c})/\sigma(W^- + c)$ cross section ratio can be used to further constrain the strange quark PDF, and to probe the level of asymmetry between the s and $\bar{s}$ PDFs [2–4].

Furthermore, the production of W + c events provides a useful calibration sample for the measurements and searches at the LHC involving electroweak bosons and c quarks in the final state [5,6]. Precise measurements of W + c production can be used to check the theoretical calculations of this process and its modeling in the currently available Monte Carlo (MC) event generators.

The W + c production in pp collisions at the LHC has been reported by the CMS [7–9], ATLAS [10,11], and LHCb [12] Collaborations at center-of-mass energies $\sqrt{s} = 7$, 8, and 13 TeV. Measurements of W + c fiducial cross sections and the $R_c^{\pm}$ cross section ratio were performed in those analyses by identifying charm events through the reconstruction of exclusive decays of charm hadrons, or finding secondary vertices or muons inside a jet.

In this paper, we present a measurement of the W + c production cross section and cross section ratio $R_c^{\pm}$ at $\sqrt{s} = 13$ TeV using the data collected in 2016–2018. The precision is improved compared with previous CMS measurements. In particular, the uncertainty in the $R_c^{\pm}$ measurement is halved, reaching a precision of 1%. Measurements are performed in four independent channels, depending on the method used for identifying the c quarks and the W boson decay mode (electron or muon). Jets are tagged as originating from the hadronization of c quarks (c jet) by the presence of either muons or secondary vertices inside the jets. The combination of the measurements in the four channels, the use of the large data set collected at $\sqrt{s} = 13$ TeV, and the reduction of systematic uncertainties, lead to more precise measurements.

A key property of W + c production is the opposite sign of the electric charges of the W boson and c quark. This feature allows the suppression of most of the background events, which exhibit bottom or charm quarks and antiquarks with equal probability and identical kinematics, such as top quark-antiquark or W + $c\bar{c}$ production. The statistical subtraction of the distributions of physical observables for events where

* e-mail: cms-publication-committee-chair@cern.ch (corresponding author)

Published online: 10 January 2024

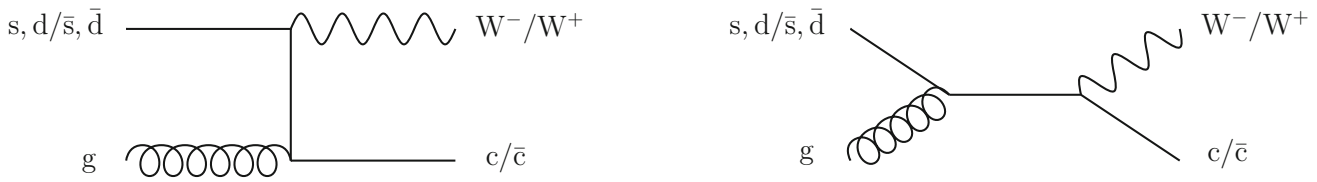

Fig. 1 Leading order Feynman diagrams for the associated production of a W boson and a charm quark. The electric charges of the W boson and c quark have opposite signs

the reconstructed charges of the W boson and the c quark have opposite sign (OS) and same sign (SS) leads to the effective removal of these backgrounds [7,8]. This technique, referred to as OS-SS subtraction, enhances the sensitivity to the sg $\to$ W + c process, and therefore to the strange quark PDF.

The OS-SS cross sections $\sigma(\mathrm{W}^+ + \bar{\mathrm{c}}) \equiv \sigma(\mathrm{pp} \to \mathrm{W}^+ + \bar{\mathrm{c}})\mathcal{B}(\mathrm{W}^+ \to \ell^+\nu)$, $\sigma(\mathrm{W}^- + \mathrm{c}) \equiv \sigma(\mathrm{pp} \to \mathrm{W}^- + \mathrm{c})\mathcal{B}(\mathrm{W}^- \to \ell^-\bar{\nu})$ (where $\mathcal{B}$ denotes the branching fraction), their sum $\sigma(\mathrm{W}+\mathrm{c}) \equiv \sigma(\mathrm{W}^+ + \bar{\mathrm{c}}) + \sigma(\mathrm{W}^- + \mathrm{c})$, and the cross section ratio $R_{\mathrm{c}}^{\pm} \equiv \sigma(\mathrm{W}^+ + \bar{\mathrm{c}})/\sigma(\mathrm{W}^- + \mathrm{c})$ are measured. Inclusive and differential cross sections are measured as functions of the transverse momentum (p_{T}^{ℓ}) and pseudorapidity (η^{ℓ}) of the lepton from the W boson decay. Measurements are unfolded to the particle and parton levels both in a fiducial region of phase space defined in terms of the kinematics of the lepton from the W boson ($p_{\mathrm{T}}^{\ell} > 35\,\mathrm{GeV}$, $|\eta^{\ell}| < 2.4$) and of the c jet ($p_{\mathrm{T}}^{\mathrm{c\,jet}} > 30\,\mathrm{GeV}$, $|\eta^{\mathrm{c\,jet}}| < 2.4$).

The theoretical cross section for W + c production at the LHC [13] is well known at the next-to-leading order (NLO) accuracy in perturbative quantum chromodynamics (QCD). Recently, the first computation of next-to-NLO (NNLO) QCD corrections was published [14,15]. The measurements presented here are compared with the predictions of these NNLO QCD calculations, which include NLO electroweak (EW) corrections. The measurements are also compared with the predictions of the parton-level MC program MCFM [16], which implements calculations at NLO in QCD using several proton PDF sets.

The paper is structured as follows: the CMS detector is briefly described in Sect. 2, and the data and simulated samples used are presented in Sect. 3. Sections 4 and 5 describe the physics object reconstruction and the selection of the W + c signal sample. Section 6 reviews the most important sources of systematic uncertainties and their impact on the measurements. Cross section and cross section ratio measurements, compared with the NLO QCD theoretical predictions using different PDF sets, are detailed in Sect. 7. The comparisons of the measurements with the NNLO QCD calculations are presented in Sect. 8. The main results of the paper are summarized in Sect. 9.

Tabulated results are provided in HEPData [17].

2 The CMS detector

The central feature of the CMS apparatus is a superconducting solenoid of 6 m internal diameter, providing a magnetic field of 3.8 T. Within the magnetic volume are a silicon pixel and strip tracker, a lead tungstate crystal electromagnetic calorimeter (ECAL), and a brass and scintillator hadron calorimeter (HCAL), each composed of a barrel and two endcap sections. Additional forward calorimetry complements the coverage provided by the barrel and endcap detectors. The silicon tracker measures charged particles within the pseudorapidity range $|\eta| < 2.5$. For nonisolated particles of $1 < p_{\mathrm{T}} < 10\,\mathrm{GeV}$ and $|\eta| < 1.4$, the track resolutions are typically 1.5% in p_{T} and 20–75 μm in the transverse impact parameter [18]. The upgrade of the pixel tracking detector [19] in early 2017, which includes additional layers and places the innermost layer closer to the interaction point, significantly improves the performance of heavy-flavor jet identification [20]. Muons are measured in the pseudorapidity range $|\eta| < 2.4$, with detection planes made using three technologies: drift tubes, cathode strip chambers, and resistive plate chambers. A more detailed description of the CMS detector, together with a definition of the coordinate system used and the relevant kinematic variables, is reported in Ref. [21].

Events of interest are selected using a two-tiered trigger system. The first level, composed of custom hardware processors, uses information from the calorimeters and muon detectors to select events at a rate of around 100 kHz within a fixed latency of about 4 μs [22]. The second level, known as the high-level trigger, consists of a farm of processors running a version of the full event reconstruction software optimized for fast processing, and reduces the event rate to around 1 kHz before data storage [23].

3 Data and simulated samples

This analysis is performed using a data sample of pp collisions at $\sqrt{s} = 13\,\mathrm{TeV}$ collected by the CMS experiment during the 2016 ($36.3\,\mathrm{fb}^{-1}$), 2017 ($41.5\,\mathrm{fb}^{-1}$), and 2018 ($59.8\,\mathrm{fb}^{-1}$) data-taking periods with a total integrated luminosity of $138\,\mathrm{fb}^{-1}$.

The experimental signature of the signal events, an isolated high-p_T lepton together with a c jet, is also present in other background processes. Sources of background include top quark production ($t\bar{t}$ and single top quark), diboson (WW, WZ, and ZZ) processes (collectively denoted as VV), the production of a Z boson (or a virtual photon) in association with jets (Z + jets), and W + $c\bar{c}$ or W + $b\bar{b}$ events.

Samples of signal and background events are simulated using MC event generators based on fixed-order perturbative QCD calculations, supplemented with parton showering and multiparton interactions. Simulated samples of W + jets and Z + jets events are produced at NLO accuracy with the MADGRAPH5_aMC@NLO [24] (version 2.6.3) matrix element generator with up to two partons in the final state. The decay of the W and Z bosons to tau leptons is included in the W + jets and Z + jets simulations. Samples of $t\bar{t}$ and single top (s-, t-, and tW channels) events are generated at NLO accuracy with POWHEG v2.0 [25]. The cross sections for W + jets, Z + jets, $t\bar{t}$, and single top production are obtained at NNLO in QCD [26,27]. The diboson production is modeled with samples of events generated with PYTHIA8 [28] (version 8.219).

The simulated W + jets sample is composed of W bosons accompanied by jets originating from quarks of all flavors and gluons. Simulated W + jets events are classified according to the flavor of the outgoing generated partons as: (i) W + b if at least one bottom quark was generated in the hard process; (ii) W + c if a single charm quark was created in the hard process; (iii) W + $c\bar{c}$ if a $c\bar{c}$ pair was present in the event; (iv) W + udsg if no c or b quarks were produced.

Data collected in different running periods are modeled with specific simulation configurations. For simulations corresponding to 2016 detector conditions, the NLO NNPDF3.0 [29] PDF set is used, whereas the MC samples for 2017–2018 make use of the NNLO NNPDF3.1 [30] PDF set. The parton showering, hadronization, and the underlying events are modeled by PYTHIAv8.212 (v8.230) using the CUETP8M1 [31,32] (CP5 [33]) tune for the 2016 (2017–2018) samples. The jet matching and merging scheme for the MADGRAPH5_aMC@NLO samples is FxFx [34].

In the PYTHIA8 simulations, the charm fragmentation fractions, defined as the probabilities for c quarks to hadronize as particular charm hadrons, corresponding to $D^{\pm}$, $D^0/\bar{D}^0$, $D_s^{\pm}$ and $\Lambda_c^{\pm}$ hadrons, are corrected to match those in Ref. [35]. In addition, the leptonic and hadronic decay branching fractions of those hadrons are corrected to agree with more recent measurements [36].

Generated events are processed through a full GEANT4-based [37] CMS detector simulation and trigger emulation. Simulated events are reconstructed with the same algorithms used to reconstruct collision data.

The simulated samples incorporate additional pp interactions in the same or nearby bunch crossings (pileup) to reproduce the experimental conditions. Simulated events are weighted so the pileup distribution matches the experimental data.

4 Object reconstruction

The global event reconstruction (also called particle-flow event reconstruction [38]) reconstructs and identifies each individual particle in an event, with an optimized combination of all subdetector information. In this process, the identification of the particle type (photon, electron, muon, charged or neutral hadron) plays an important role in the determination of the particle direction and energy. Photons are identified as ECAL energy clusters not linked to the extrapolation of any charged-particle trajectory. Electrons are identified as a primary charged-particle track and with many ECAL energy clusters corresponding to this track extrapolation to the ECAL and to possible bremsstrahlung photons emitted along the path through the tracker material. Muons are identified as tracks in the central tracker consistent with either a track or several hits in the muon system, and associated with calorimeter deposits compatible with the muon hypothesis. Charged hadrons are identified as charged particle tracks neither identified as electrons nor as muons. Finally, neutral hadrons are identified as HCAL energy clusters not linked to any charged-hadron trajectory, or as a combined ECAL and HCAL energy excess with respect to the expected charged-hadron energy deposit.

The primary vertex (PV) is taken to be the vertex corresponding to the hardest scattering in the event, evaluated using tracking information alone, as described in Section 9.4.1 of Ref. [39].

The energy of photons is obtained from the ECAL measurement. The energy of electrons is determined from a combination of the track momentum at the PV, the corresponding ECAL cluster energy, and the energy sum of all bremsstrahlung photons associated with the track. The energy of muons is obtained from the corresponding track momentum. The energy of charged hadrons is determined from a combination of the track momentum and the corresponding ECAL and HCAL energies, corrected for the response function of the calorimeters to hadronic showers. Finally, the energy of neutral hadrons is obtained from the corresponding corrected ECAL and HCAL energies.

The electron momentum is estimated by combining the energy measurement in the ECAL with the momentum measurement in the tracker. The momentum resolution for electrons with $p_T \approx 45$ GeV from $Z \to ee$ decays ranges from 1.6 to 5.0%. It is generally better in the barrel region than in the endcaps, and also depends on the bremsstrahlung energy emitted by the electron as it traverses the material in front of the ECAL [40,41]. Matching muons to tracks measured in

the silicon tracker results in a p_T resolution of 1% in the barrel and 3% in the endcaps for muons with p_T up to 100 GeV [42].

For each event, hadronic jets are clustered from these reconstructed particles using the infrared- and collinear-safe anti-k_T algorithm [43,44] with a distance parameter of 0.4. The jet momentum is determined as the vector sum of all particle momenta in the jet, and is found from simulation to be, on average, within 5–10% of the true momentum over the entire p_T spectrum and detector acceptance. Pileup interactions can contribute additional tracks and calorimetric energy depositions to the jet momentum. To mitigate this effect, charged particles identified as originating from pileup vertices are discarded, and an offset correction is applied to correct for remaining contributions from neutral particles. Jet energy corrections are derived from simulation to bring the measured response of jets to that of particle level jets on average. In situ measurements of the momentum balance in dijet, photon + jet, Z + jet, and multijet events are used to account for any residual differences in the jet energy scale (JES) between data and simulation [45]. The jet energy resolution (JER) amounts typically to 15–20% at 30 GeV, 10% at 100 GeV, and 5% at 1 TeV. Additional selection criteria are applied to each jet to remove jets potentially dominated by anomalous contributions from various subdetector components or reconstruction failures.

The missing transverse momentum vector $\vec{p}_T^{\,miss}$ is the projection on the plane perpendicular to the beams of the negative vector momenta sum of all particles that are reconstructed with the particle-flow algorithm. The $\vec{p}_T^{\,miss}$ is modified to account for corrections to the energy scale of the reconstructed jets in the event. The missing transverse momentum, p_T^{miss}, is defined as the magnitude of the $\vec{p}_T^{\,miss}$ vector, and it is a measure of the transverse momentum of particles leaving the detector undetected [46].

The trigger, reconstruction, and selection efficiencies are corrected in simulations to match those observed in the data. Lepton efficiencies (ϵ_ℓ) are evaluated with data samples of dilepton events in the Z boson mass peak with the tag-and-probe method [47], and correction factors $\epsilon_\ell^{data}/\epsilon_\ell^{MC}$, binned in p_T^ℓ and η^ℓ of the leptons, are implemented.

5 Event selection

Events with a high-p_T lepton from the decay of a W boson are selected online by a trigger algorithm that requires the presence of an electron (muon) candidate with minimum p_T of 27, 32, and 32 GeV (24, 27, and 24 GeV) during the 2016, 2017, and 2018 data-taking periods, respectively. Electrons and muons are selected using tight identification criteria following the reconstruction algorithms discussed in Refs. [40,42]. The analysis follows the selection strategy used in Ref. [8] and requires the presence of a high-p_T isolated lepton in the region $|\eta^\ell| < 2.4$ and $p_T^\ell > 35$ GeV.

The combined isolation variable, I_{comb}, quantifies additional hadronic activity around the selected leptons. It is defined as the sum of the transverse momenta of neutral hadrons, photons, and charged hadrons in a cone with $\Delta R = \sqrt{(\Delta\eta)^2 + (\Delta\phi)^2} < 0.3$ (0.4) around the electron (muon) candidate, excluding the contribution from the lepton itself, where ϕ is the azimuthal angle in radians. Only charged particles originating from the PV are included in the sum to minimize the contribution from pileup interactions. The contribution of neutral particles from pileup vertices is estimated and subtracted from I_{comb}. For electrons, this contribution is evaluated with the jet area method described in Ref. [48]; for muons, it is assumed to be half the p_T sum of all charged particles in the cone originating from pileup vertices. The factor one-half accounts for the expected ratio of neutral to charged particle production in hadronic interactions. The lepton candidate is considered to be isolated if $I_{comb}/p_T^\ell < 0.15$. Events with an additional isolated lepton with $p_T^\ell > 20$ GeV are rejected to suppress the contribution from Z + jets and $t\bar{t}$ events.

The transverse mass (m_T) of the lepton and $\vec{p}_T^{\,miss}$ is defined as,

$$m_T \equiv \sqrt{2\, p_T^\ell\, p_T^{miss}\, [1 - \cos(\phi_\ell - \phi_{p_T^{miss}})]},$$

where ϕ_ℓ and $\phi_{p_T^{miss}}$ are the azimuthal angles of the lepton and the $\vec{p}_T^{\,miss}$ vector. Events with $m_T < 55$ GeV are discarded from the analysis to suppress the contamination from events composed uniquely of jets produced through the strong interaction, referred to as QCD multijet events. The contribution of this background was evaluated with two methods: (i) using a QCD multijet simulation; and (ii) by means of data control regions, inverting the selection requirements in transverse mass and lepton isolation to infer the contribution in the signal region. The contamination after OS-SS subtraction is negligible.

In addition to the requirements that select events with a W boson, we require the presence of at least one jet with $p_T^{jet} > 30$ GeV and $|\eta^{jet}| < 2.4$. Jets with an angular separation between the jet axis and the selected isolated lepton $\Delta R(\text{jet}, \ell) < 0.4$ are not considered.

5.1 Identification of charm jets

Hadrons with b and c quark content decay through the weak interaction with lifetimes of the order of 10^{-12} s and mean decay lengths larger than 100 μm at the energies relevant for this analysis. Secondary vertices well separated from the PV can be identified and reconstructed from the charged particle tracks. In a sizeable fraction of the heavy-flavor hadron decays (≈10–15% [36]) there is a muon in the final state. We

make use of these properties to define two independent data samples enriched with jets originating from a c quark: (i) the semileptonic (SL) channel, where a muon coming from the semileptonic decay of a c hadron is identified inside a jet; and (ii) the secondary vertex (SV) channel, where a displaced SV is reconstructed inside a jet. The charge of the c quark is determined from the charge of the muon in the SL channel, and the charges of the SV tracks in the SV case, as described in more detail below.

If an event fulfills both the SL and SV selection requirements (about 6% of the selected events), it is assigned to the SL channel. Thus, the SL and SV channels are mutually exclusive, i.e., the samples selected in each channel are statistically independent.

These two signatures also feature weakly decaying b hadrons. Events from processes involving the associated production of W bosons and b quarks are abundantly selected in the two categories. The dominant background contribution stems from $\mathrm{t\bar{t}}$ production, where a pair of W bosons and two b jets are produced in the decays of the top quark-antiquark pair. This final state mimics the analysis topology when at least one of the W bosons decays leptonically and one of the b jets contains an identified muon or a reconstructed SV. However, this background is effectively suppressed by the OS-SS subtraction. A $\mathrm{t\bar{t}}$ event will be categorized as OS (SS) when the lepton from the W decay and the muon or SV from the b quark are coming from the same (different) top quark. The probability of identifying a muon or an SV inside the b (or $\bar{\mathrm{b}}$) jet with opposite or same charge as the charge of the W candidate is expected to be the same, thus producing an equal amount of OS and SS events.

Top quark-antiquark events where one of the W bosons decays hadronically into a $\mathrm{c\bar{s}}$ (or $\bar{\mathrm{c}}\mathrm{s}$) pair may result in additional event candidates if the SL or SV signature originates from the c jet. This topology produces genuine OS events, which contribute to the remaining background contamination after OS-SS subtraction. Similarly, single top quark production also produces OS events, but at a lower level because of the smaller production cross section. These remaining background contributions after OS-SS subtraction are estimated with simulations and are subtracted in the cross section measurements.

The production of a W boson and a single bottom quark through the process $\mathrm{qg} \to \mathrm{W} + \mathrm{b}$, similar to the one sketched in Fig. 1, produces OS events, but it is heavily Cabibbo-suppressed and its contribution is negligible. The other source of a W boson and a b quark is $\mathrm{W} + \mathrm{b\bar{b}}$ events where the $\mathrm{b\bar{b}}$ pair originates from a gluon splitting mechanism. These events are also charge-symmetric, since it is equally likely to identify the b jet with the same or opposite charge than that of the W boson. This contribution also cancels out after the OS-SS subtraction. The same argument applies to $\mathrm{W} + \mathrm{c\bar{c}}$ events.

5.1.1 Event selection in the SL channel

The W + c events with a semileptonic c quark decay are selected by requiring a reconstructed muon among the constituents of any of the selected jets. Semileptonic c quark decays into electrons are not considered because of a high background in identifying electrons inside jets. The muon candidate must satisfy the same reconstruction and identification quality criteria as those imposed on the muons from the W boson decay, except for isolation, and must be reconstructed in the region $|\eta| < 2.4$, with $p_{\mathrm{T}}^{\mu} < 25\,\mathrm{GeV}$ and $p_{\mathrm{T}}^{\mu}/p_{\mathrm{T}}^{\mathrm{jet}} < 0.6$. The p_{T} requirements reduce the contamination from prompt muons overlapping with or misreconstructed as jets. No minimum p_{T} threshold is explicitly required, but the muon reconstruction algorithm sets a natural threshold of around 3 (2) GeV in the barrel (endcap) region since the muon must traverse the material in front of the muon detector and penetrate deep enough into the muon system to be reconstructed and satisfy the identification criteria. If more than one such muon is identified, the one with the highest p_{T} is selected.

Additional requirements are applied for the event selection in the $\mathrm{W} \to \mu\nu$ channel, since the selected sample is affected by a sizeable contamination from dimuon Z + jets events, where one of the muons from the Z decay is reconstructed inside a jet. The track of the muon coming from a semileptonic decay of a charm hadron tends to have a considerable transverse impact parameter with respect to the PV. We require the transverse impact parameter significance (IPS) of the muon in the jet, defined as the muon transverse impact parameter divided by its uncertainty, to be larger than 2. In addition, events with a dimuon invariant mass close to the Z boson mass peak ($70 < m_{\mu\mu} < 110\,\mathrm{GeV}$) are discarded. Furthermore, $m_{\mu\mu}$ must be larger than 12 GeV to suppress the background from low-mass resonances.

The normalizations of the $\mathrm{t\bar{t}}$ and Z + jets backgrounds are derived from data control samples. A Z + jets data control sample is defined using the same selection criteria as the analysis but inverting the $m_{\mu\mu}$ requirement to select events close to the Z boson mass peak ($70 < m_{\mu\mu} < 110\,\mathrm{GeV}$). A normalization factor of 1.08 ± 0.01 is required to match the Z + jets simulation with data. The $\mathrm{t\bar{t}}$ data control sample is established by selecting events with the same requirements as the analysis and additionally demanding at least three high-p_{T} jets, two of which are tagged as b jets (using the loose working point of the DeepCSV b-tagging algorithm [49]), and the remaining jet contains a muon. A normalization factor of 0.92 ± 0.02 is required to bring into agreement data and $\mathrm{t\bar{t}}$ simulation. The uncertainty in the background normalization factors reflects the statistical uncertainty of the data and the simulations in the control samples. Once the absolute normalization of the Z + jets and $\mathrm{t\bar{t}}$ background contri-

Table 1 Data and background event yields (with statistical uncertainties) after selection and OS-SS subtraction for the SL channels (electron and muon W decay modes)

SL channel	Data	Background
$W \to e\nu$	424 047 ± 1286	80 646 ± 933
$W \to \mu\nu$	263 669 ± 918	68 108 ± 917

butions are determined, the W + jets simulation is scaled so that the sum of the events from all predicted contributions be equal to the number of events in the selected data sample. The normalization factor of the W + jets simulation (0.95) has only a minor effect in the contribution of the (small) predicted W + udsg background. The overall normalization of the W+c signal simulation is irrelevant for the analysis, since it is only used for acceptance and efficiency calculations.

Events are classified as OS or SS depending on the electric charges of the lepton from the W boson decay and the muon inside the jet.

Table 1 shows the event yields in the $W \to e\nu$ and $W \to \mu\nu$ channels after the selection requirements described above and after OS-SS subtraction. The $W \to \mu\nu$ channel has a significantly lower yield due to the additional requirements to reduce the sizeable Z+jets background. The background yields, as estimated with the simulations, are also included in the table. The signal and background composition of the selected sample according to simulation is shown in Table 2. The fraction of signal W+c events in the $W \to e\nu$ channel is above 80%, whereas in the $W \to \mu\nu$ channel it drops to 74% because of the additional Z + jets background (around 6%). The dominant background, $t\bar{t}$ production, where one of the W bosons decays leptonically and the other hadronically with a charm quark in the final state, amounts to approximately 10%.

Figure 2 shows the p_T distributions of the muon inside the jet (upper) and of the lepton from the W decay (lower), for events in the selected SL sample, after the background normalization corrections described above. The simulations agree with the data within uncertainties.

5.1.2 Event selection in the SV channel

An independent W + c sample is selected by looking for secondary decay vertices of charmed hadrons within the reconstructed jets. Displaced SVs are reconstructed with either the simple secondary vertex (SSV) [50] or the inclusive vertex finder (IVF) [51,52] algorithms. Both algorithms follow the adaptive vertex fitter technique [53] to construct an SV, but differ in the track selection used. The SSV algorithm takes as input the tracks constituting the jet, whereas the IVF algorithm starts from a displaced track with respect to the PV (seed track) and tries to build a vertex from nearby tracks in terms of their separation distance in three dimensions and their angular separation around the seed track. The IVF vertices are then associated to the closest jet in a cone of $\Delta R = 0.3$. Both SSV and IVF vertices always start with input tracks with a minimum p_T of 1 GeV to minimize the effects from poorly reconstructed tracks. Vertices reconstructed with the IVF algorithm are considered first. If no IVF vertex is found, SSV vertices are searched for, thus providing additional event candidates (about 3%). If more than one SV is reconstructed within a jet, the one with the highest p_T, computed from its associated tracks, is selected. If there are several jets with an SV, only the SV associated to the jet of highest p_T is selected.

At least three tracks must be associated with an SV for it to be considered. This requirement largely reduces the contamination of jets coming from the hadronization of light-flavor quarks (u, d, and s) or gluons. It also reduces the systematic uncertainty associated with the SV reconstruction efficiency. To ensure that the SV is well separated from the PV, we require the displacement significance, defined as the three dimensional distance between the PV and SV, divided by its uncertainty, to be larger than 8. This requirement suppresses the W + udsg background contribution below 1%.

To classify the event as OS or SS, we measure the sign of the charge of the charm quark produced in the hard interaction. For charged charm hadrons, the sum of the charges of the decay products reflects the charge of the c quark. For neutral charm hadrons, the charge of the closest hadron produced in the fragmentation process can indicate the charge of the c quark [54,55]. Hence, we assign a charge equal to the sum of the charges of the particle tracks associated with the SV. If the SV charge is zero, we assume the charge of the track that is closest in angular separation to the SV. We only consider PV tracks with $p_T > 0.3$ GeV and within an angular separation from the SV direction of 0.1 in the (η, ϕ) space. If nonzero charge cannot be assigned, the event is rejected. According to the simulation, the charge assignment proce-

Table 2 Simulated signal and background composition (in percentage) of the SL sample after selection and OS-SS subtraction. The $W + Q\bar{Q}$ stands for the sum of the contributions of $W + c\bar{c}$ and $W + b\bar{b}$

SL channel	W + c	$W + Q\bar{Q}$	W + udsg	Z + jets	$t\bar{t}$	Single t	VV
$W \to e\nu$	81.0 ± 0.6	0.5 ± 0.3	3.1 ± 0.5	0.4 ± 0.1	10.0 ± 0.1	4.4 ± 0.1	0.6 ± 0.1
$W \to \mu\nu$	74.2 ± 0.5	0.5 ± 0.3	2.0 ± 0.4	5.5 ± 0.2	11.6 ± 0.1	5.8 ± 0.1	0.4 ± 0.1

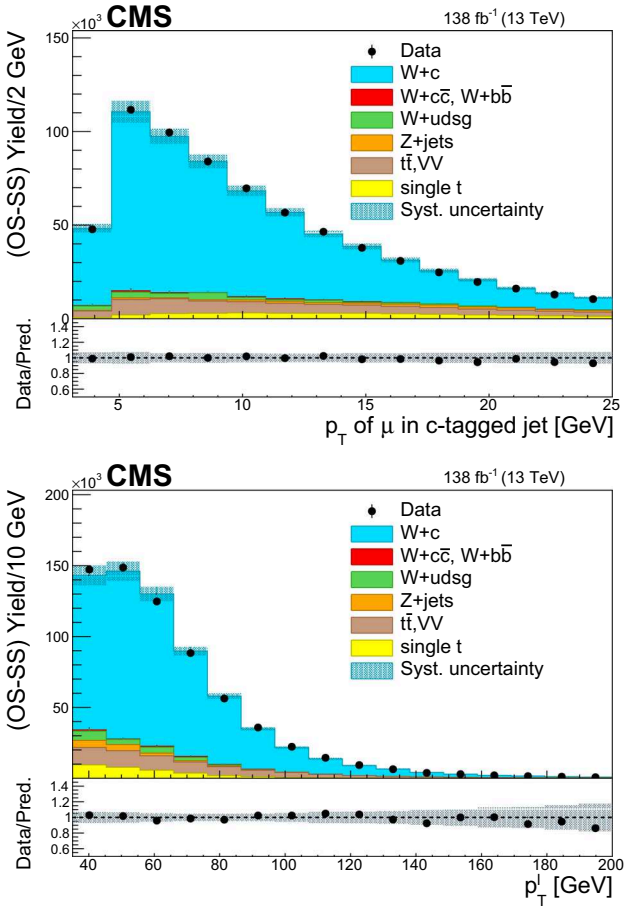

Fig. 2 Distributions after OS-SS subtraction of the p_T of the muon inside the c jet (upper) and the p_T of the lepton from the W decay (lower) for events in the SL sample, summing up the contributions of the W boson decay channels to electrons and muons. The contributions of the various processes are estimated with the simulated samples. The statistical uncertainty in the data is smaller than the size of the data dots. The hatched areas represent the sum in quadrature of statistical and systematic uncertainties in the MC simulation. The ratio of data to simulation is shown in the lower panels. The uncertainty band in the ratio includes the statistical uncertainty in the data, and the statistical and systematic uncertainties in the MC simulation

dure provides a nonzero charge for 99% of the selected SVs, and the sign of the charge is correctly assigned in 83% of the cases.

The modeling of the SV charge assignment in the simulation has been validated with data. Events passing both the SL and SV selection criteria are used to compare the charges of the muon inside the jet and the SV. In 95% of these events the charges agree. The difference in the charge assignment efficiency between data and simulation, around 1%, is taken as a systematic uncertainty in the cross section measurements, as detailed in Sect. 6.

The SV reconstruction efficiency in the simulation is calibrated using data. The events of the SL sample are used to compute data-to-simulation scale factors for the efficiency

Table 3 Data and background event yields (with statistical uncertainties) after selection and OS-SS subtraction for the SV channels (electron and muon W decay modes)

SV channel	Data	Background
$W \to e\nu$	$338\,504 \pm 1717$	$60\,565 \pm 1577$
$W \to \mu\nu$	$494\,264 \pm 1876$	$94\,356 \pm 2002$

of charm identification through the reconstruction of an SV [5,49]. The fraction of events in the SL sample with an SV is computed for data and simulation, and the ratio of data to simulation is applied as a scale factor to the simulated W + c signal events in the SV sample. The calculated scale factor is 0.93 ± 0.03, where the uncertainty accounts for statistical and systematic effects. The systematic uncertainty includes contributions from uncertainties in the pileup description, JES and JER, lepton efficiencies, background subtraction, and modeling of charm production and decay fractions in the simulation.

Table 3 shows the event yields in the $W \to e\nu$ and $W \to \mu\nu$ channels after the selection requirements and OS-SS subtraction. The background yields, as estimated with the simulations, are also included. The contributions of the backgrounds were rescaled using the normalization factors described in Sect. 5.1.1. The signal and background composition of the selected sample, as predicted by the simulation, are shown in Table 4. The purity of signal W + c events is above 80%. The dominant backgrounds come from $t\bar{t}$ (8%) and single top (9%) production.

The event selection requirements are summarized in Table 5 for the four selection channels of the analysis, the W boson decay channels to both electrons or muons, and the SL and SV charm identification channels.

Figure 3 shows the distributions, after OS-SS subtraction, of the corrected SV mass and the SV transverse momentum divided by the jet transverse momentum, p_T^{SV}/p_T^{jet}. The latter is a representative observable of the energy fraction of the charm quark carried by the charm hadron in the fragmentation process. We define the corrected SV mass, m_{SV}^{corr}, as the invariant mass of all charged particles associated with the SV, assumed to be pions, m_{SV}, corrected for additional particles, either charged or neutral, that may have been produced but were not reconstructed [56]:

$$m_{SV}^{corr} = \sqrt{m_{SV}^2 + p_{SV}^2 \sin^2\theta} + p_{SV} \sin\theta,$$

where p_{SV} is the modulus of the vectorial sum of the momenta of all charged particles associated with the SV, and θ is the angle between the momentum vector sum and the vector from the PV to the SV. The corrected SV mass is thus the minimum mass the long-lived hadron can have that is consistent with the direction of its momentum.

Table 4 Simulated signal and background composition (in percentage) of the SV sample after selection and OS-SS subtraction. The $W + Q\bar{Q}$ stands for the sum of the contributions of $W + c\bar{c}$ and $W + b\bar{b}$

SV channel	$W + c$	$W + Q\bar{Q}$	$W + udsg$	$Z + jets$	$t\bar{t}$	Single t	VV
$W \to e\nu$	82.1 ± 0.8	0.7 ± 0.4	1.0 ± 0.6	0.1 ± 0.2	7.2 ± 0.1	8.4 ± 0.1	0.5 ± 0.1
$W \to \mu\nu$	80.9 ± 0.6	0.7 ± 0.3	0.5 ± 0.4	0.5 ± 0.2	8.0 ± 0.1	8.9 ± 0.1	0.5 ± 0.1

Table 5 Summary of the selection requirements for the four selection channels of the analysis

	SL $W \to e\nu$	SL $W \to \mu\nu$	SV $W \to e\nu$	SV $W \to \mu\nu$
Lepton p_T^{ℓ}	>35 GeV			
Lepton $\lvert\eta^{\ell}\rvert$	<2.4			
Lepton isolation I_{comb}/p_T^{ℓ}	<0.15			
Transverse mass m_T	>55 GeV			
Jet p_T^{jet}	>30 GeV			
Jet $\lvert\eta^{jet}\rvert$	<2.4			
$\Delta R(\text{jet}, \ell)$	>0.4			
Muon in jet p_T^{μ}	<25 GeV			
Muon in jet p_T^{μ}/p_T^{jet}	<0.6			
Muon in jet $\lvert\eta^{\mu}\rvert$	<2.4			
Muon in jet IPS		>2		
Muon in jet $m_{\mu\mu}$		>12 GeV & $\notin[70, 110$ GeV$]$		
SV number of tracks			>2	
SV displacement significance			>8	
SV charge			$\neq 0$	

The normalization of the single top quark background is fixed with data. Single top quark events populate the tail of the m_{SV}^{corr} distribution. A normalization factor of 1.5 ± 0.2 for the single top quark contribution was required to match data and simulation predictions. The same rescaling is applied to the SL and SV samples.

6 Systematic uncertainties

The impact of various sources of uncertainty in the measurements presented in Sect. 7 is estimated by recalculating the cross sections with the relevant parameters varied up and down by one standard deviation of their uncertainties.

The combined uncertainty in the trigger, reconstruction, and identification efficiencies for isolated leptons results in an uncertainty in the cross section measurements of about 2% (1%) for the $W \to e\nu$ ($W \to \mu\nu$) channel. The uncertainty in the identification efficiency of nonisolated muons inside jets is approximately 3%, according to dedicated studies with $Z+$jets events. This uncertainty affects only the SL channel.

The effects of the uncertainty in the JES and JER are assessed by varying up and down the p_T values of jets with the corresponding uncertainty factors. The JES and JER uncertainties are also propagated to $\vec{p}_T^{\,miss}$. The resulting uncertainty in the cross section is about 2% (1%) for the SL (SV) channel. The uncertainty from a $\vec{p}_T^{\,miss}$ mismeasurement in the event is estimated by varying within its uncertainty the contribution of the energy unassociated with reconstructed particle-flow objects. The effect in the cross section measurement is $<0.5\%$. Uncertainties in the pileup modeling are calculated using a modified pileup profile obtained by changing the mean number of interactions by $\approx 5\%$. This variation covers the uncertainty in the pp inelastic cross section [57] and in the modeling of the pileup simulation. It results in less than 0.5% uncertainty in the cross section measurements.

The integrated luminosities of the 2016, 2017, and 2018 data-taking periods are individually known with uncertainties in the 1.2–2.5% range [58–60], whereas the total 2016–2018 integrated luminosity has an uncertainty of 1.6%. The improvement in precision arises from the (uncorrelated) time evolution of some systematic effects.

The uncertainty in the scale factor correcting the SV reconstruction efficiency in the simulation propagates into a systematic uncertainty of 3% in the cross section. The uncertainty in the SV charge determination is estimated as the difference (1%) in the rate obtained in data and simulation of correct SV charge assignment in the validation test described in Sect. 5.1.2.

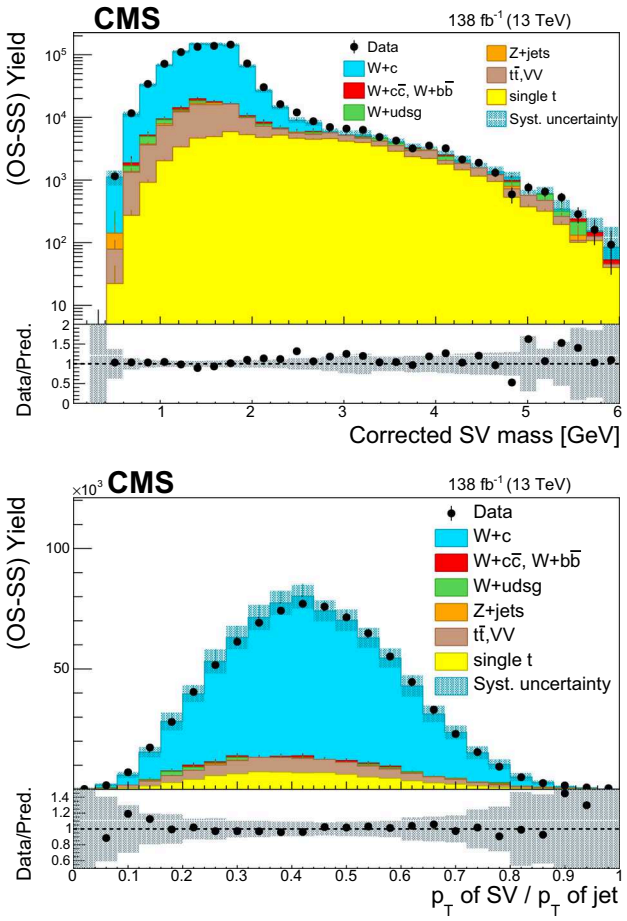

Fig. 3 Distributions after OS-SS subtraction of the corrected SV mass (upper) and SV transverse momentum divided by the jet transverse momentum (lower) for events in the SV sample, summing up the contributions of the W boson decay channels to electrons and muons. The contributions from all processes are estimated with the simulated samples. The statistical uncertainty in the data is smaller than the size of the data dots for most of the data points. The hatched areas represent the sum in quadrature of statistical and systematic uncertainties in the MC simulation. The ratio of data to simulation is shown in the lower panels. The uncertainty band in the ratio includes the statistical uncertainty in the data, and the statistical and systematic uncertainties in the MC simulation

Because of the dependence of the SV reconstruction efficiency on the SV displacement, we have evaluated the effect produced by an imperfect modeling of this observable by reweighting the SV displacement significance distribution of the simulation to match that of the data. The resulting uncertainty in the cross section measurement is 1–2%. In addition, the stability of the results with the minimum SV displacement significance requirement was checked by changing the threshold from 8 to 7. The effect in the results is also at the 1% level.

The background contributions are evaluated with the simulations validated in data control samples, as discussed in Sect. 5.1.1. The uncertainty in the predicted background levels has an effect of 1% in the cross section measurements.

The signal samples used for the acceptance and efficiency calculations were generated with MADGRAPH+ PYTHIA8 using the NNPDF3.0 and NNPDF3.1 PDF sets. The envelope of the systematic variations (replicas) of the nominal PDF is assumed to be the systematic uncertainty due to an imperfect knowledge of the PDFs, as recommended in Ref. [61]. The effect is approximately 1%. The statistical uncertainty in the determination of the selection efficiency using the simulated samples is 1%, and is propagated as an additional systematic uncertainty.

In the signal and background modeling, no uncertainty is included in the simulation of higher-order terms in perturbative QCD (parton shower). The OS-SS subtraction technique removes the contribution to W + c production coming from charm quark-antiquark pair production, rendering the measurement insensitive to this effect. The uncertainty in the modeling of the hard process in the signal simulation is assessed by independently changing the QCD factorization and renormalization scales by factors of 0.5 and 2 relative to the nominal value. The resulting uncertainty in the cross section measurement is negligible.

To estimate the effect produced by the uncertainties in the corrected values used in the simulation for the charm fragmentation and decay branching fractions [35,36], we have varied those values within their uncertainties. The impact in the cross section measurements is 1–2%, both for the fragmentation and decay branching fractions.

The main systematic uncertainties are summarized in Table 6 for the four selection channels of the analysis. Overall, the total systematic uncertainty in the W + c fiducial cross section is approximately 5% in all channels.

7 Cross section measurements

The W + c production cross section measurements are restricted to a phase space region that is close to the experimental fiducial volume with optimized sensitivity for the signal process. Cross sections are measured inclusively within the fiducial phase space region and differentially as a function of p_{T}^{ℓ} and $|\eta^{\ell}|$. Cross section measurements are performed independently in four different channels, the two charm identification SL and SV channels, and the two W boson decay channels. The four measurements are combined to improve the precision.

Measurements are unfolded to the particle and parton levels. At both levels, the fiducial region is defined by a lepton at the generator level coming from the decay of a W boson with $p_{\mathrm{T}}^{\ell} > 35$ GeV and $|\eta^{\ell}| < 2.4$, together with a generator-level

Table 6 Summary of the main systematic uncertainties, in percentage of the measured fiducial cross section, for the four selection channels of the analysis

Source	SL $W \to e\nu$	SL $W \to \mu\nu$	SV $W \to e\nu$	SV $W \to \mu\nu$
	Uncertainty [%]			
Isolated lepton identification	1.6	0.9	1.6	0.9
Jet energy scale and resolution	2.0	2.0	1.0	1.0
Muon in jet identification	3.0	3.0	–	–
SV reconstruction	–	–	3.7	3.7
Charm fragmentation and decay	2.6	2.6	2.4	2.4
PDF in MC samples	1.0	1.0	1.0	1.0
Stat. uncert. selection efficiency	0.9	1.2	0.9	0.8
Background contributions	0.6	0.9	1.3	1.3
Integrated luminosity	1.6	1.6	1.6	1.6
Total	5.2	5.1	5.4	5.2

c jet with $p_{\mathrm{T}}^{\mathrm{c\ jet}} > 30\,\mathrm{GeV}$ and $|\eta^{\mathrm{c\ jet}}| < 2.4$. The OS-SS subtraction is also applied at generator level. This removes the charge-symmetric contributions that mostly originate from gluon splitting into a charm quark-antiquark pair. The c jet must be well separated from the lepton by an angular distance $\Delta R(\mathrm{c\ jet}, \ell) > 0.4$. Jets at the generator level are clustered using the anti-k_{T} jet algorithm with a distance parameter $R = 0.4$. At the particle level, jets are formed using generator particles produced after the hadronization process. At the parton level, jets are constructed from the hard interaction partons.

For all channels under study, the W + c cross section is determined using the following expression:

$$\sigma(\mathrm{W}+\mathrm{c}) = \frac{Y_{\mathrm{sel}} - Y_{\mathrm{bkg}}}{\mathcal{C}\,\mathcal{L}}, \tag{1}$$

where Y_{sel} is the selected OS-SS event yield, and Y_{bkg} the background yield in data after OS-SS subtraction, estimated from simulation and normalized using the data control samples described in Sect. 5.1. $\mathcal{L}$ is the integrated luminosity of the data sample.

The factor $\mathcal{C}$ corrects for acceptance and efficiency losses in the selection process of W + c events produced in the fiducial region at the generator level. It also subtracts the contributions from W+c events outside the kinematic region of the measurements and from W + c events with $W \to \tau\nu$, $\tau \to e + X$ or $\tau \to \mu + X$. It is calculated, using the sample of simulated signal events, as the ratio between the event yield of the selected W + c sample (according to the procedure described in Sects. 5.1.1 and 5.1.2 and after OS-SS subtraction) and the number of OS-SS W+c events satisfying the phase space definition at the generator level. Independent correction factors $\mathcal{C}$ are computed at the particle and parton levels, and for the four selection channels.

Table 7 Measured production cross sections $\sigma(\mathrm{W}+\mathrm{c})$ unfolded to the particle level in the four selection channels together with statistical (first) and systematic (second) uncertainties. The acceptance times efficiency values ($\mathcal{C}$) are also given

Channel	$\mathcal{C}$(%)	$\sigma(\mathrm{W}+\mathrm{c})$ [pb]
$W \to e\nu$, SL	$1.568 \pm 0.014 \pm 0.077$	$158.7 \pm 0.6 \pm 8.3$
$W \to \mu\nu$, SL	$0.946 \pm 0.011 \pm 0.044$	$149.8 \pm 0.7 \pm 7.7$
$W \to e\nu$, SV	$1.389 \pm 0.013 \pm 0.068$	$145.0 \pm 0.9 \pm 7.6$
$W \to \mu\nu$, SV	$1.966 \pm 0.015 \pm 0.093$	$147.4 \pm 0.7 \pm 7.5$

7.1 Measurements at the particle level

Cross section measurements, unfolded to the particle level, are presented in this section. The fiducial W + c production cross section measurements computed with Eq. (1) for the four channels separately are shown in Table 7, together with the event yields and the $\mathcal{C}$ correction factors. The different $\mathcal{C}$ values reflect the different reconstruction and selection efficiencies in the four channels. In the SL channel, less than 5% of the signal charm hadrons generated in the fiducial region of the analysis produce a muon in their decay with enough momentum to reach the muon detector and get reconstructed. Similarly, in the SV channel, less than 5% of the events with a charm hadron decay remain after SV reconstruction, SV charge assignment, and OS-SS subtraction. The remaining inefficiency, accounted for in the $\mathcal{C}$ correction factor, is due to the selection requirements of the samples.

Results obtained for the W + c cross sections in the four different channels are consistent within the uncertainties, and are combined using the best linear unbiased estimator method [62] that takes into account individual uncertainties and their correlations. Systematic uncertainties arising from a common source and affecting several measurements are consid-

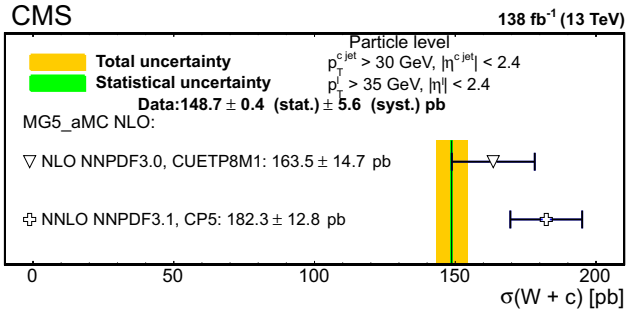

Fig. 4 Comparison of the measured fiducial $\sigma(\mathrm{W}+\mathrm{c})$ cross section unfolded to the particle level with the predictions from the MADGRAPH5_aMC@NLO simulation using two different PDF sets (NLO NNPDF3.0 and NNLO NNPDF3.1). Two different tunes (CUETP8M1 and CP5) for the parton showering, hadronization and underlying event modeling in PYTHIA8 are also used. Horizontal error bars indicate the total uncertainty in the predictions

ered as fully correlated. In particular, all systematic uncertainties are assumed fully correlated between the electron and muon channels, except those related to the lepton reconstruction. The χ^2 of the combination is 4.8 (three degrees of freedom), corresponding to a p-value of 0.19. The combined measured cross section unfolded to the particle level is:

$$\sigma(\mathrm{W}+\mathrm{c}) = 148.7 \pm 0.4\,(\mathrm{stat}) \pm 5.6\,(\mathrm{syst})\,\mathrm{pb}.$$

Measurements are compared with the predictions of the MADGRAPH5_aMC@NLO MC generator, as shown in Fig. 4. In the predictions, two different NNPDF PDF sets (versions 3.0 and 3.1) are used. The two predictions differ as well in the tune used in PYTHIA8 for the parton showering, hadronization, and underlying event modeling (CUETP8M1 and CP5). The predicted cross sections are about 10% (using NLO NNPDF3.0) and 20% (NNLO NNPDF3.1) higher than the measured value, with relative uncertainties close to 10%. The uncertainty associated with the MC predictions includes the uncertainties associated with the renormalization and factorization scales, as well as the uncertainty related to the PDFs used in the simulation. The scale uncertainties are estimated using a set of weights provided by the generator that corresponds to independent variations of the scales by factor of 0.5, 1, and 2. The prediction is obtained for all combinations (excluding the cases where one scale is reduced and the other is increased at the same time) and their envelope is quoted as the uncertainty. The uncertainty in the PDFs is estimated using different Hessian eigenvectors of each PDF set.

The $\sigma(\mathrm{W}+\mathrm{c})$ production cross section is also measured differentially as a function of $|\eta^{\ell}|$ and p_{T}^{ℓ}. The total sample is divided into subsamples according to the value of $|\eta^{\ell}|$ or p_{T}^{ℓ}, and the cross section is computed using Eq. (1). The binning of the differential distributions is chosen such that each bin is sufficiently populated to perform the measurement. Event migration between neighbouring bins caused by detector resolution effects is evaluated with the simulated signal sample and is negligible. Measurements in the four channels are combined assuming that systematic uncertainties are fully correlated among bins of the differential distributions.

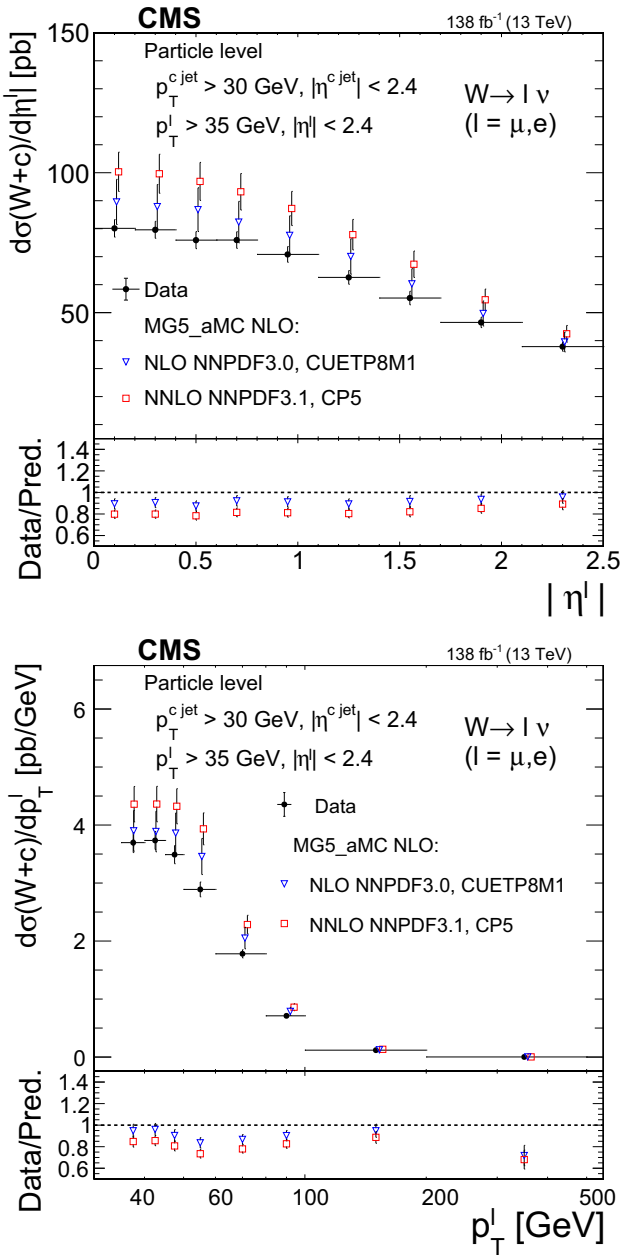

Fig. 5 Measured differential cross sections $\mathrm{d}\sigma(\mathrm{W}+\mathrm{c})/\mathrm{d}|\eta^{\ell}|$ (upper) and $\mathrm{d}\sigma(\mathrm{W}+\mathrm{c})/\mathrm{d}p_{\mathrm{T}}^{\ell}$ (lower) unfolded to the particle level, compared with the predictions of the MADGRAPH5_aMC@NLO simulation. Two different PDF sets (NLO NNPDF3.0 and NNLO NNPDF3.1) are used. Error bars on data points include statistical and systematic uncertainties. Symbols showing the theoretical expectations are slightly displaced in the horizontal axis for better visibility. The ratios of data to predictions are shown in the lower panels. The uncertainty in the ratio includes the uncertainties in both data and prediction

Table 8 Measured production cross sections $\sigma(\mathrm{W}+\mathrm{c})$ unfolded to the parton level in the four selection channels together with statistical (first) and systematic (second) uncertainties. The acceptance times efficiency values ($\mathcal{C}$) are also given

Channel	$\mathcal{C}$(%)	$\sigma(\mathrm{W}+\mathrm{c})$ [pb]
$\mathrm{W}\to\mathrm{e}\nu$, SL	$1.419 \pm 0.012 \pm 0.069$	$175.3 \pm 0.7 \pm 9.2$
$\mathrm{W}\to\mu\nu$, SL	$0.856 \pm 0.010 \pm 0.040$	$165.4 \pm 0.8 \pm 8.5$
$\mathrm{W}\to\mathrm{e}\nu$, SV	$1.261 \pm 0.012 \pm 0.062$	$159.6 \pm 1.0 \pm 8.4$
$\mathrm{W}\to\mu\nu$, SV	$1.786 \pm 0.014 \pm 0.084$	$162.3 \pm 0.8 \pm 8.2$

Systematic uncertainties in the differential $\sigma(\mathrm{W}+\mathrm{c})$ cross section measurements are in the range of 4–6%. The main sources of systematic uncertainty, as discussed in Sect. 6, are related to the charm hadron fragmentation and decay fractions in the simulation (2%), and the efficiency of identifying an SV or a muon inside a jet (3%).

The $\sigma(\mathrm{W}+\mathrm{c})$ differential cross section as a function of $|\eta^{\ell}|$ and p_{T}^{ℓ}, obtained after the combination of the measurements in the SL, SV, electron, and muon channels, is shown in Fig. 5, compared with the predictions from the MADGRAPH5_aMC@NLO simulation. Observed shape differences are within 10%.

7.2 Measurements at the parton level

The measurements are also unfolded to the parton level, including an additional correction to account for the c quark fragmentation and hadronization processes. Results of the fiducial cross sections in the four selection channels are presented in Table 8. The combination of the measurements is:

$$\sigma(\mathrm{W}+\mathrm{c}) = 163.4 \pm 0.5\,(\mathrm{stat}) \pm 6.2\,(\mathrm{syst})\,\mathrm{pb}.$$

The fiducial cross section measured at the parton level is expected to be slightly larger than that at the particle level. During the hadronization and jet clustering processes, the momentum of the c quark gets smeared and biased towards slightly smaller values. A fraction of charm quarks near the $p_{\mathrm{T}}^{\mathrm{c}} > 30\,\mathrm{GeV}$ threshold of the fiducial region of the measurement do not result in c jets with $p_{\mathrm{T}}^{\mathrm{c\,jet}} > 30\,\mathrm{GeV}$. On the other hand, a number of W + c events with a c quark with $p_{\mathrm{T}}^{\mathrm{c}} < 30\,\mathrm{GeV}$ get reconstructed with a generator level jet with $p_{\mathrm{T}}^{\mathrm{c\,jet}} > 30\,\mathrm{GeV}$. The net effect is the the observed reduction of about 10% of the cross section at the particle level.

The measurements unfolded to the parton level are compared with analytical calculations of W + c production. We have used the MCFM 9.1 program [16] to evaluate the cross section predictions in the phase space of the analysis: $p_{\mathrm{T}}^{\ell} > 35\,\mathrm{GeV}$, $|\eta^{\ell}| < 2.4$, $p_{\mathrm{T}}^{\mathrm{c\,jet}} > 30\,\mathrm{GeV}$, and $|\eta^{\mathrm{c\,jet}}| < 2.4$. Jets are clustered in MCFM using the anti-k_{T} jet algorithm with a distance parameter $R = 0.4$. The W+c process description is available in MCFM up to $\mathcal{O}(\alpha_{\mathrm{S}}{}^2)$ with a massive charm quark ($m_{\mathrm{c}} = 1.5\,\mathrm{GeV}$). The contributions from gluon splitting into $\mathrm{c\bar{c}}$ are not included. We have computed predictions for the following NLO PDF sets: MSHT20 [63], CT18 [64], CT18Z [64], ABMP16 [65], NNPDF3.0 [29], and NNPDF3.1 [30]. The LHAPDF6 library [66] was used to access the PDF sets. All of the PDF sets were derived using strangeness-sensitive experimental data, including LHC W/Z and jet production cross section measurements. The NNPDF and MSHT20 sets additionally incorporate the CMS W + c production at $\sqrt{s} = 7\,\mathrm{TeV}$ data. CTA18Z differs from CTA18 because the former includes the ATLAS W/Z 7 TeV precision measurements [67] leading to an enhancement of the strange PDF. The PDF parameterizations of the MSHT20 and NNPDF groups allow for strangeness asymmetry.

The factorization and the renormalization scales are set to the value of the W boson mass [36]. The uncertainty from missing higher perturbative orders is estimated by computing cross section predictions varying independently the factorization and renormalization scales to twice and half their nominal values, with the constraint that the ratio of scales is never larger than 2. The envelope of the resulting cross sections with these scale variations defines the theoretical scale uncertainty. The value in the calculation of the strong coupling constant at the energy scale of the mass of the Z boson, $\alpha_{\mathrm{S}}(m_{\mathrm{Z}})$, is set to the recommended values by each of the PDF groups. Uncertainties in the predicted cross sections associated with $\alpha_{\mathrm{S}}(m_{\mathrm{Z}})$ are evaluated as half the difference in the predicted cross sections evaluated with a variation of $\Delta(\alpha_{\mathrm{S}}) = \pm 0.002$.

The theoretical predictions for the fiducial W+c cross section in the phase space of the measurements are summarized in Table 9. The central value of the prediction is provided together with the relative uncertainties arising from the PDF variations within each set, the choice of scales, and α_{S}. The size of the PDF uncertainties depends on the different input data and methodology used by the various groups. In particular, they depend on the parameterization of the strange quark PDF and on the definition of the one standard deviation uncertainty band. The maximum difference between the central values of the various PDF predictions is ∼10%. This difference is comparable to the total uncertainty in each of the individual predictions. Theoretical predictions are slightly larger than the measured cross section but are in agreement within the uncertainties, as depicted in Fig. 6.

Table 9 Predictions for $\sigma(\mathrm{W}+\mathrm{c})$ production from MCFM at NLO in QCD for the phase space of the analysis. For every PDF set, the central value of the prediction is given, together with the uncertainty as prescribed from the PDF set, and the uncertainties associated with the scale variations and with the value of α_S. The total uncertainty is given in the last column. The last row in the table gives the experimental result presented in this paper

PDF set	$\sigma(\mathrm{W}+\mathrm{c})$ [pb]	Δ_{PDF} [pb]	Δ_{scales} [pb]	Δ_{α_S} [pb]	Total uncert. [pb]
MSHT20	176.3	$^{+6.8}_{-6.3}$	$^{+6.8}_{-7.4}$	±0.01	$^{+9.6}_{-9.7}$
CT18	164.9	$^{+11.1}_{-8.7}$	$^{+6.1}_{-6.8}$	$^{+0.9}_{-0.8}$	$^{+12.7}_{-11.1}$
CT18Z	176.4	$^{+13.5}_{-10.5}$	$^{+7.0}_{-7.4}$	$^{+0.6}_{-0.5}$	$^{+15.2}_{-12.8}$
ABMP16	183.6	±3.3	$^{+7.2}_{-7.8}$	$^{+1.5}_{-0.9}$	$^{+7.9}_{-8.4}$
NNPDF3.0	161.9	±6.2	$^{+5.8}_{-6.7}$	±0.01	$^{+8.5}_{-9.1}$
NNPDF3.1	175.2	±6.1	$^{+6.6}_{-7.3}$	±0.01	$^{+9.1}_{-9.5}$

CMS: $163.4 \pm 0.5\,(\mathrm{stat}) \pm 6.2\,(\mathrm{syst})$ pb

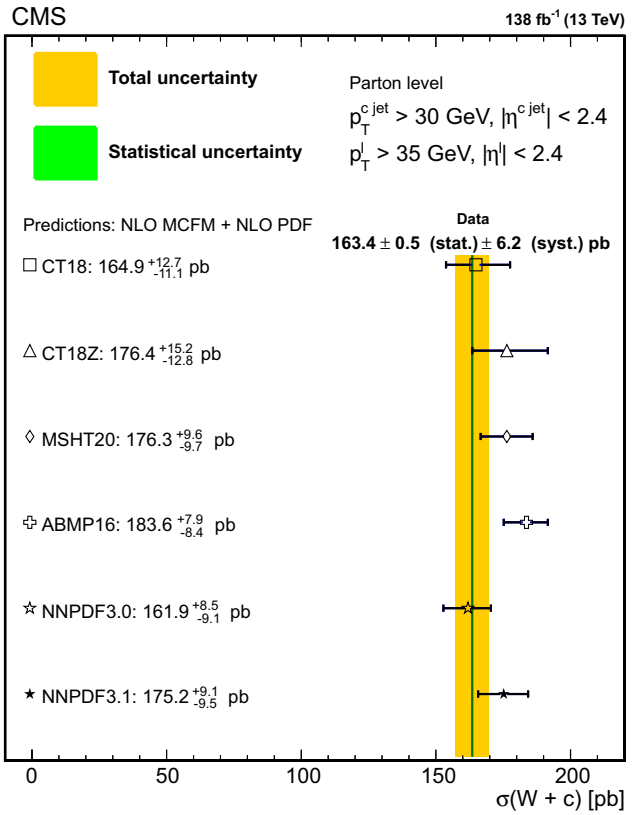

Fig. 6 Comparison of the experimental measurement of $\sigma(\mathrm{W}+\mathrm{c})$, unfolded to the parton level, with the predictions from the NLO QCD MCFM calculations using different NLO PDF sets. Horizontal error bars indicate the total uncertainty in the predictions

The predictions for the $\sigma(\mathrm{W}+\mathrm{c})$ production cross section, computed in intervals of $|\eta^{\ell}|$ and p_{T}^{ℓ}, are compared with the measured values in Fig. 7. The predictions are generally consistent with the measurements within uncertainties, except for the highest p_{T}^{ℓ} bin.

7.3 Measurements of the cross section ratio $\sigma(\mathrm{W}^+ + \bar{\mathrm{c}})/\sigma(\mathrm{W}^- + \mathrm{c})$

The cross section ratio $\sigma(\mathrm{W}^+ + \bar{\mathrm{c}})/\sigma(\mathrm{W}^- + \mathrm{c})$ is measured in the four channels as the ratio of the OS-SS event yields in which the lepton from the W boson decay is positively or negatively charged:

$$R_{\mathrm{c}}^{\pm} = \frac{\sigma(\mathrm{W}^+ + \bar{\mathrm{c}})}{\sigma(\mathrm{W}^- + \mathrm{c})} = \frac{Y_{\mathrm{sel}}^{+} - Y_{\mathrm{bkg}}^{+}}{Y_{\mathrm{sel}}^{-} - Y_{\mathrm{bkg}}^{-}}. \quad (2)$$

The OS-SS background contributions, Y_{bkg}^{+} and Y_{bkg}^{-}, estimated with the simulations, are subtracted from the selected event yields Y_{sel}^{+} and Y_{sel}^{-}. The statistical uncertainty in the background contributions in the four analysis channels is treated as a source of systematic uncertainty (0.5–0.8%) in the cross section ratio.

Most of the reconstruction and selection efficiencies cancel out in the measurement of the cross section ratio $R_{\mathrm{c}}^{\pm}$. Possible efficiency differences between positive and negative leptons and SVs are included as systematic uncertainties. We evaluate effects stemming from charge confusion and charge-dependent reconstruction efficiencies.

The probability of assigning the incorrect charge to a lepton is studied with data using $\mathrm{Z} \to \ell\ell$ events reconstructed with SS or OS leptons. For the muons, the charge misidentification probability is negligible ($< 10^{-3}$). For the electrons, the effect is around 1% but propagates into a negligible uncertainty in the cross section ratio. The charge confusion rate for the SVs is significantly larger, 17%, as described in Sect. 5.1.2. However, assuming that the charge confusion probability is the same for positive and negative SVs, the effect in the cross section ratio cancels out.

Potential differences in the reconstruction efficiencies of positive and negative leptons or SVs are studied with the $\mathrm{W}+\mathrm{c}$ MC simulation. Efficiency ratios are calculated independently for the four channels of the analysis and are consistent with unity within the statistical uncertainty (1.2–1.4%).

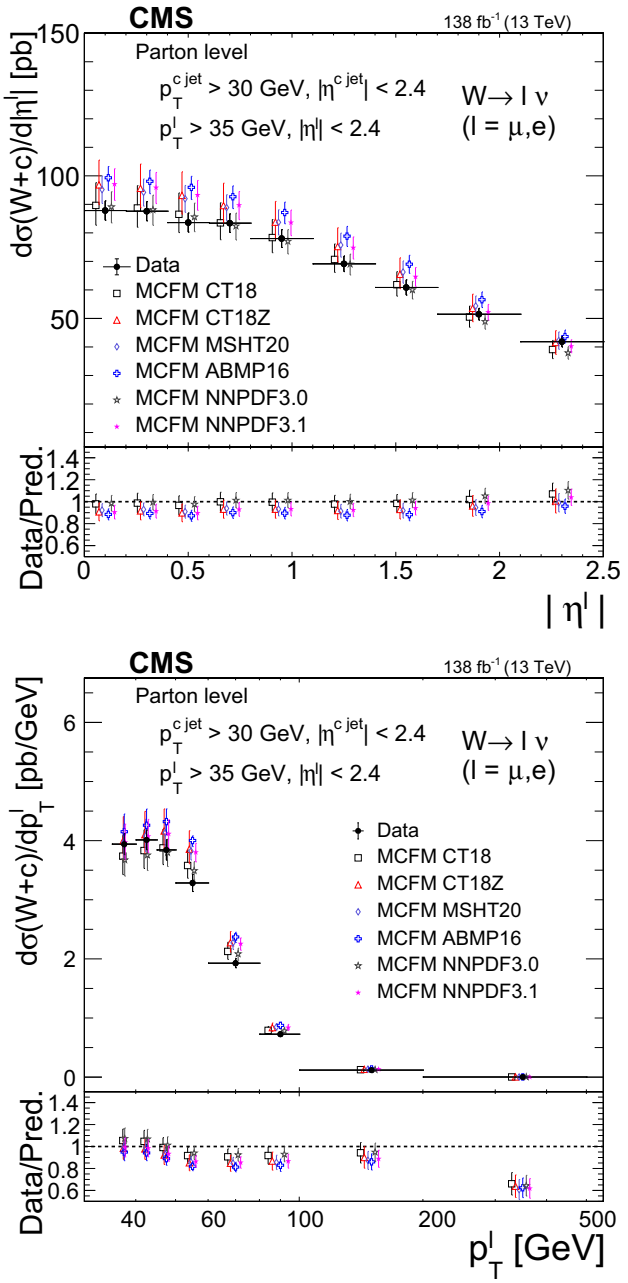

Fig. 7 Measured differential cross sections $\mathrm{d}\sigma(\mathrm{W}+\mathrm{c})/\mathrm{d}|\eta^{\ell}|$ (upper) and $\mathrm{d}\sigma(\mathrm{W}+\mathrm{c})/\mathrm{d}p_{\mathrm{T}}^{\ell}$ (lower) unfolded to the parton level, compared with the predictions from the MCFM NLO calculations using different NLO PDF sets. Error bars on data points include statistical and systematic uncertainties. Symbols showing the theoretical expectations are slightly displaced in the horizontal axis for better visibility. The ratios of data to predictions are shown in the lower panels. The uncertainty in the ratio includes the uncertainties in both data and prediction

No corrections are made in the $R_{\mathrm{c}}^{\pm}$ measurements but the statistical uncertainties in the efficiency ratios are treated as systematic uncertainties.

The $R_{\mathrm{c}}^{\pm}$ measurements in the four channels are presented in Table 10. The four measurements are combined considering as fully correlated the systematic uncertainties of electron, muon and SV reconstruction efficiencies affecting several channels. The χ^2 of the combination is 3.3 (three degrees of freedom), corresponding to a p value of 0.35. The combined cross section ratio measurement is:

$$R_{\mathrm{c}}^{\pm} = 0.950 \pm 0.005\,(\mathrm{stat}) \pm 0.010\,(\mathrm{syst}).$$

The precision in the $R_{\mathrm{c}}^{\pm}$ measurement has been improved by a factor of two with respect to previous CMS measurements [7–9], leading to the most precise measurement of $R_{\mathrm{c}}^{\pm}$ to date.

In Fig. 8 the $R_{\mathrm{c}}^{\pm}$ measurement is compared with the MCFM calculations using various PDF sets. Theoretical predictions for $\sigma(\mathrm{W}^{+}+\bar{\mathrm{c}})$ and $\sigma(\mathrm{W}^{-}+\mathrm{c})$ are computed independently under the same conditions explained in Sect. 7.2 and for the same $|\eta^{\ell}|$ and p_{T}^{ℓ} ranges used in the analysis. Expectations for $R_{\mathrm{c}}^{\pm}$ are derived from them and presented in Table 11. All

Table 10 Measured production cross section ratio $R_{\mathrm{c}}^{\pm}$ in the four selection channels. Statistical (first) and systematic (second) uncertainties are also given

Channel	$R_{\mathrm{c}}^{\pm}$
$\mathrm{W} \to \mathrm{e}\nu$, SL	$0.934 \pm 0.006 \pm 0.013$
$\mathrm{W} \to \mu\nu$, SL	$0.940 \pm 0.006 \pm 0.014$
$\mathrm{W} \to \mathrm{e}\nu$, SV	$0.961 \pm 0.008 \pm 0.013$
$\mathrm{W} \to \mu\nu$, SV	$0.974 \pm 0.006 \pm 0.015$

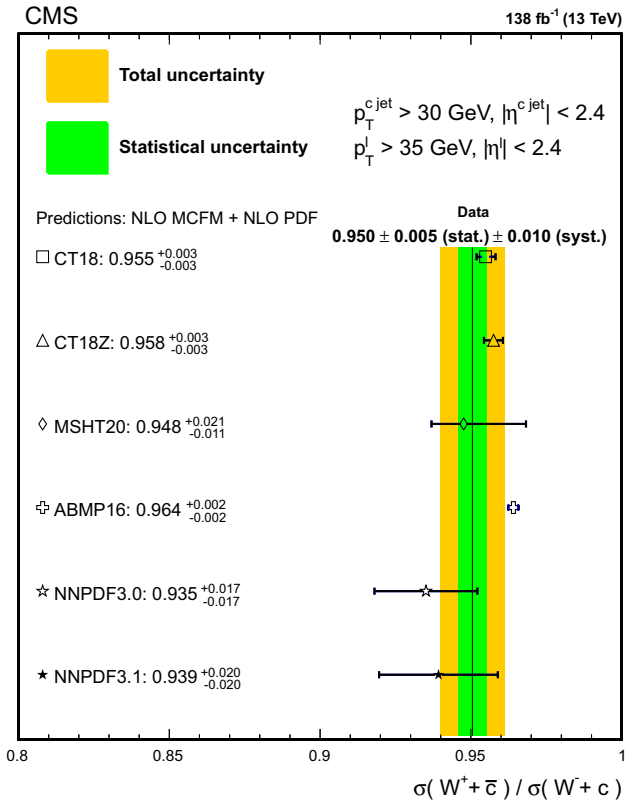

Fig. 8 Comparison of the experimental measurement of $R_{\mathrm{c}}^{\pm}$ with the NLO QCD MCFM calculations using different NLO PDF sets. Horizontal error bars indicate the total uncertainty in the predictions

Table 11 Theoretical predictions for $R_c^{\pm}$ calculated with MCFM at NLO. The kinematic selection follows the experimental requirements. For every PDF set, the central value of the prediction is given, together with the uncertainty as prescribed from the PDF set, and the uncertainties associated with the scale variations and with the value of α_S. The total uncertainty is given in the last column. The last row in the table gives the experimental result presented in this paper

PDF set	$R_c^{\pm}$	Δ_{PDF}	Δ_{scales}	Δ_{α_S}	Total uncert.
MSHT20	0.948	$^{+0.021}_{-0.011}$	± 0.001	± 0.0001	$^{+0.021}_{-0.011}$
CT18	0.955	± 0.003	± 0.003	± 0.001	± 0.003
CT18Z	0.958	± 0.003	± 0.001	± 0.001	± 0.003
ABMP16	0.964	± 0.002	± 0.001	± 0.001	± 0.002
NNPDF3.0	0.935	± 0.017	± 0.001	± 0.0001	± 0.017
NNPDF3.1	0.939	± 0.020	± 0.001	± 0.0001	± 0.020

CMS: $0.950 \pm 0.005\,(\text{stat}) \pm 0.010\,(\text{syst})$

theoretical uncertainties are significantly reduced in the cross section ratio prediction.

The $R_c^{\pm}$ observable is sensitive to a potential strangeness asymmetry in the proton but also to the down quark and antiquark asymmetry through the Cabibbo-suppressed down quark contribution to the W + c production. In the absence of strangeness asymmetry, as in the PDF sets CT18 and ABMP16, the predicted $R_c^{\pm}$ value in the kinematical region of the analysis ranges from 0.955 to 0.964 with a small uncertainty of about 0.2%. The predictions calculated using PDF sets that include strangeness asymmetry in the proton (MSHT20 and NNPDF) are about 2% lower, ranging from 0.935 to 0.948 with a 2% uncertainty as a result of the larger uncertainty associated with the difference between the strange quark and antiquark PDFs. Within experimental and theoretical uncertainties, the measured $R_c^{\pm}$ value is consistent with both sets of predictions.

The cross section ratio $R_c^{\pm}$ is also measured differentially as a function of $|\eta^{\ell}|$ and p_T^{ℓ}. The measurements are compared with the MCFM predictions in Fig. 9. The predictions are generally consistent with the measurements, with some small deviations in shape within 5%. The cross section ratio decreases with $|\eta^{\ell}|$ from $R_c^{\pm} \sim 1$ in the central region to about 0.87 for the most forward lepton pseudorapidity values. This behaviour is expected since different Bjorken x regions are being probed. At larger x values, corresponding to higher values of $|\eta^{\ell}|$, $W^- + c$ production increases relative to $W^+ + \bar{c}$ because of the growing contribution initiated by the valence down quark. The differences between the predictions made using PDF sets with and without strange quark asymmetry grow with increasing $|\eta^{\ell}|$ and p_T^{ℓ}. However, with the current uncertainties, the data cannot distinguish between both sets of predictions.

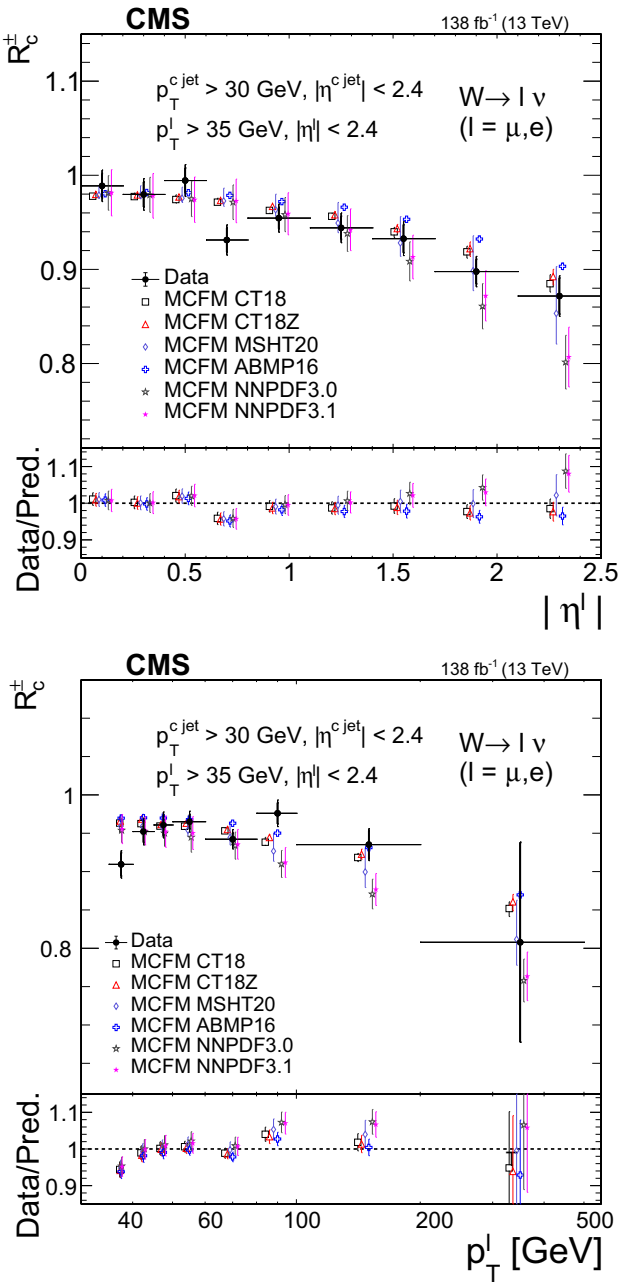

Fig. 9 Measured cross section ratio $R_c^{\pm}$ as a function of the absolute value of η^{ℓ} (upper) and p_T^{ℓ} (lower), compared with the NLO QCD MCFM calculations using different NLO PDF sets. Error bars on data points include statistical and systematic uncertainties. Symbols showing the theoretical expectations are slightly displaced in the horizontal axis for better visibility. The ratios of data to predictions are shown in the lower panels. The uncertainty in the ratio includes the uncertainties in both data and prediction

Table 12 Predictions for $\sigma(\mathrm{W}+\mathrm{c})$ in the phase space of the analysis. For each QCD and EW order, the central values of the OS, SS and OS-SS predictions are given, together with the statistical, scales, PDF, and total uncertainties of the OS-SS prediction. All values are given in pb. The last row in the table gives the experimental result presented in this paper

QCD order	EW order	$\sigma^{\mathrm{OS}}_{\mathrm{W+c}}$	$\sigma^{\mathrm{SS}}_{\mathrm{W+c}}$	$\sigma^{\mathrm{OS\text{-}SS}}_{\mathrm{W+c}}$	$\Delta^{\mathrm{OS\text{-}SS}}_{\mathrm{stat}}$	$\Delta^{\mathrm{OS\text{-}SS}}_{\mathrm{scales}}$	$\Delta^{\mathrm{OS\text{-}SS}}_{\mathrm{PDF}}$	$\Delta^{\mathrm{OS\text{-}SS}}_{\mathrm{Total}}$
LO	LO	137.4	0	137.4	±0.1	$^{+16.6}_{-13.3}$	±5.1	$^{+17.4}_{-14.3}$
NLO	LO	182.4	4.1	178.3	±0.3	$^{+9.3}_{-9.4}$	±6.8	$^{+11.6}_{-11.6}$
NNLO	LO	182.9	8.2	174.7	±1.0	$^{+1.2}_{-2.8}$	±6.8	$^{+7.0}_{-7.4}$
NNLO	NLO	179.1	8.0	171.1	±1.0	$^{+1.2}_{-2.8}$	±6.8	$^{+7.0}_{-7.4}$

CMS: $163.4 \pm 0.5\,(\mathrm{stat}) \pm 6.2\,(\mathrm{syst})$ pb

8 Comparison with predictions using NNLO QCD and NLO EW calculations

The first computation of NNLO QCD corrections for $\mathrm{W}+\mathrm{c}$ production has recently been presented [14,15]. The latest calculations include full off-diagonal CKM dependence up to NNLO QCD accuracy, and the dominant NLO EW corrections. In addition, a modified anti-k_{T} jet algorithm (flavored anti-k_{T} [68]) is used to guarantee that the computations are infrared safe. This is important for a fair comparison between theory predictions and experimental measurements, since experimental results are derived using the anti-k_{T} jet algorithm.

Predictions corresponding to the phase space of the CMS measurements presented in this paper, $p_{\mathrm{T}}^{\ell} > 35\,\mathrm{GeV}$, $|\eta^{\ell}| < 2.4$, $p_{\mathrm{T}}^{\mathrm{c\,jet}} > 30\,\mathrm{GeV}$, $|\eta^{\mathrm{c\,jet}}| < 2.4$, $\Delta R(\mathrm{jet}, \ell) > 0.4$, have been specifically computed for the purpose of this comparison, using the charge-dependent flavored anti-k_{T} jet algorithm with parameter $a = 0.1$, and the same input parameters as in Ref. [15]. The theoretical cross sections are provided at LO, NLO, and NNLO QCD accuracies. At LO, the $\mathrm{W}+\mathrm{c}$ process is defined at order $\mathcal{O}(\alpha_{\mathrm{S}}\alpha^2)$ in the strong and EW couplings. At NLO, the QCD corrections include all virtual and real contributions of order $\mathcal{O}(\alpha_{\mathrm{S}}^2\alpha^2)$. In the same way, at NNLO accuracy all double-virtual, double-real, and real-virtual contributions of order $\mathcal{O}(\alpha_{\mathrm{S}}^3\alpha^2)$ are included. The calculation is carried out in the 5-flavor scheme with massless bottom and charm quarks. NLO EW corrections of order $\mathcal{O}(\alpha_{\mathrm{S}}\alpha^3)$ are calculated including all virtual corrections and the real corrections involving single real photon emission to cancel the corresponding IR divergences appearing in the EW one-loop amplitude.

The nominal renormalization and factorization scales are set both to $\frac{1}{2}(E_{\mathrm{T,W}} + p_{\mathrm{T}}^{\mathrm{c\,jet}})$, where $E_{\mathrm{T,W}} = \sqrt{M_{\mathrm{W}}^2 + (\vec{p}_{\mathrm{T}}^{\,\ell} + \vec{p}_{\mathrm{T}}^{\,\nu})^2}$. To estimate missing higher-order QCD corrections, the scale uncertainty is obtained by independently varying the two scales by factors of 0.5, 1, 2, and taking the envelope of the predictions obtained with all variations excluding the cases where one scale is reduced and the other is increased at the same time.

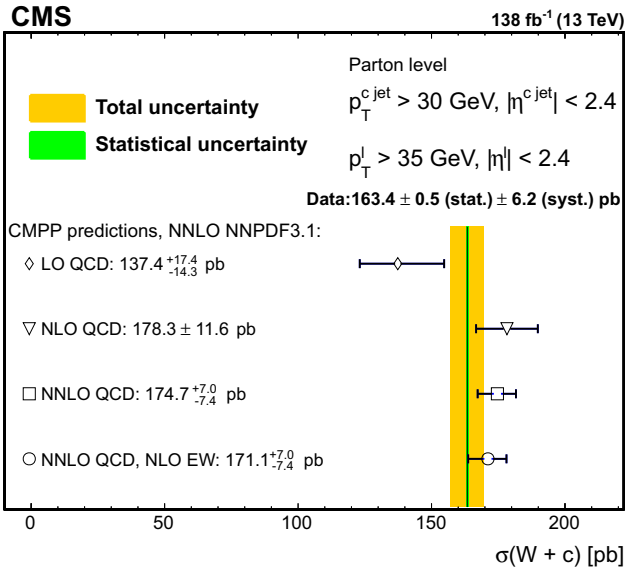

Fig. 10 Comparison of the experimental measurement of $\sigma(\mathrm{W}+\mathrm{c})$ with the OS-SS LO, NLO, and NNLO QCD predictions, and NLO EW corrections. The NNLO QCD NNPDF3.1 PDF set is used for computing all the predictions. CMPP stands for the authors of the calculations [15]. Horizontal error bars indicate the total uncertainty in the predictions

The calculation was performed for the most representative PDF set, which allows for strange asymmetry, NNPDF3.1. The NNLO QCD PDF set was used for computing the predictions for all orders, following the PDF4LHC recommendation [61]. To evaluate the PDF uncertainty of the NNPDF3.1 sets, specialized minimal PDF sets [69], which contain only 8 replicas, were used. The PDF uncertainty is calculated as the square root of the quadratic sum of the differences between the cross section obtained with the nominal PDF and that obtained with each replica.

In Table 12, the theoretical predictions for the OS, SS, and OS-SS inclusive fiducial cross section are given at LO, NLO, and NNLO QCD accuracies. The QCD corrections show good perturbative convergence, since the NNLO QCD corrections are significantly smaller than the NLO ones. The NNLO correction for the OS-SS cross section is negative, about -2%. This occurs becausse the NNLO QCD corrections to SS are larger than those for OS; at LO there is no SS

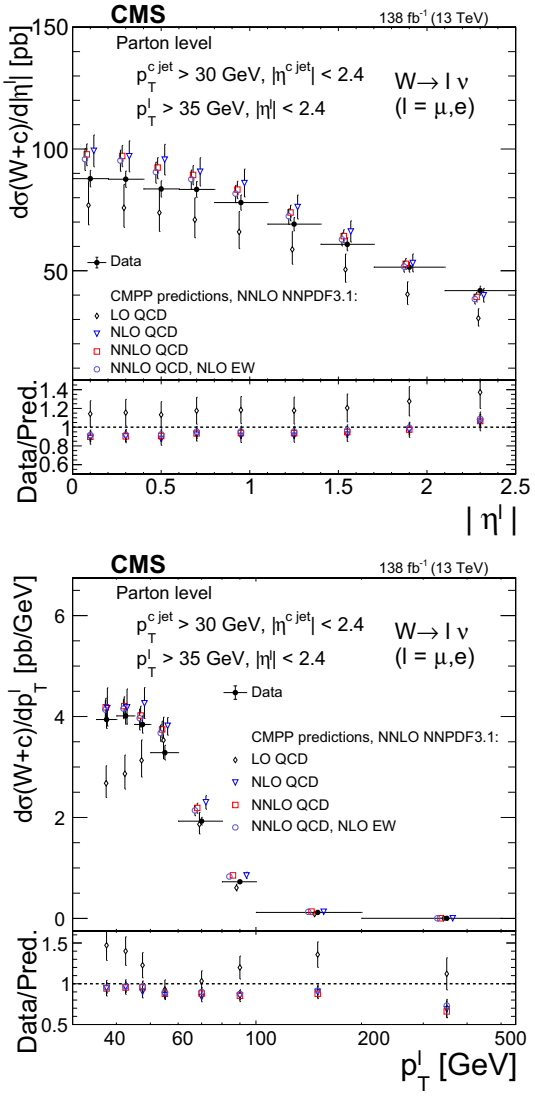

Fig. 11 Comparison of the measured differential cross sections $\mathrm{d}\sigma(\mathrm{W}+\mathrm{c})/\mathrm{d}|\eta^{\ell}|$ (upper) and $\mathrm{d}\sigma(\mathrm{W}+\mathrm{c})/\mathrm{d}p_{\mathrm{T}}^{\ell}$ (lower) with the OS-SS LO, NLO, and NNLO QCD predictions, and NLO EW corrections. The NNLO QCD NNPDF3.1 PDF set is used for computing all the predictions. CMPP stands for the authors of the calculations [15]. Error bars on data points include statistical and systematic uncertainties. Symbols showing the theoretical expectations are slightly displaced in the horizontal axis for better visibility. The ratios of data to predictions are shown in the lower panels. The uncertainty in the ratio includes the uncertainties in both data and prediction

contribution to the W+c process and the first SS contribution enters at NLO. The cross section calculated at NNLO QCD including NLO EW corrections is also shown in Table 12. The EW corrections amount to -2%. They were included as a multiplicative factor with negligible statistical uncertainty.

At LO and NLO the total uncertainty in the predictions is dominated by the scale uncertainty (around 5% at NLO). At NNLO the scale uncertainty is reduced to 1%, and the PDF uncertainty (4%) dominates. The inclusion of NNLO QCD corrections provides a more precise determination of the strange quark content of the proton from the cross section observable.

Table 13 Theoretical predictions for $R_{\mathrm{c}}^{\pm}$. For each QCD order, the central values are given, together with the MC statistical, scales, PDF, and total uncertainties. The last row in the table gives the experimental result presented in this paper

QCD order	$R_{\mathrm{c}}^{\pm}$	Δ_{stat}	Δ_{scales}	Δ_{PDF}	Δ_{Total}
LO	0.945	$\pm$0.001	$\pm$0.001	$\pm$0.022	$\pm$0.022
NLO	0.939	$\pm$0.004	$\pm$0.002	$\pm$0.023	$\pm$0.023
NNLO	0.936	$\pm$0.011	$\pm$0.002	$\pm$0.023	$\pm$0.026

CMS: $0.950 \pm 0.005\,(\mathrm{stat}) \pm 0.010\,(\mathrm{syst})$

The OS-SS predictions are compared with the fiducial cross section measurement in Fig. 10. The OS-SS subtraction reduces the NNLO corrections, but does not remove them completely. The inclusion of the NNLO corrections decreases the uncertainty in the prediction and also brings it closer to the experimental measurement. The EW NLO corrections further improves the agreement between the theoretical prediction and experimental data. The theoretical prediction and the experimental measurement agree within uncertainties.

No efficiency correction has been applied to account for the different flavor assignments in the jet algorithms of the predictions (flavored anti-k_{T}) and the experimental measurements (anti-k_{T}). In Ref. [15] the difference in the predictions from the standard anti-k_{T} and the flavored anti-k_{T} algorithms is studied. Due to the lack of flavored infrared safety for the standard anti-k_{T} algorithm, such a comparison can be done only at NLO with the help of a parton shower. The difference in the fiducial cross section predictions is below 1%. Similarly, the effect in the NNLO theoretical W + c cross section prediction using variations of the flavored anti-k_{T} algorithm, and the flavored k_{T} algorithm is studied. Differences are also below 1%.

The predictions are also compared with the differential cross section measurements $\mathrm{d}\sigma(\mathrm{W}+\mathrm{c})/\mathrm{d}|\eta^{\ell}|$ and $\mathrm{d}\sigma(\mathrm{W}+\mathrm{c})/\mathrm{d}p_{\mathrm{T}}^{\ell}$ in Fig. 11. The NLO correction is approximately flat in $|\eta^{\ell}|$ while it is larger at low and high values of p_{T}^{ℓ}. The NLO predictions are very similar to those shown in Fig. 7 calculated with MCFM at NLO using the same PDF set (NNPDF3.1). The NNLO correction is small and does not change the shape of the NLO predictions. The EW NLO correction is flat in $|\eta^{\ell}|$ and gets larger with p_{T}^{ℓ}, from 0.99 in the first bin to 0.90 in the highest p_{T}^{ℓ} bin.

Predictions for the OS-SS cross section ratio $R_{\mathrm{c}}^{\pm}$ have also been computed and are collected in Table 13. In computing the scale variation of $R_{\mathrm{c}}^{\pm}$, the scale uncertainty for the positive and negative signatures is taken as correlated. The $R_{\mathrm{c}}^{\pm}$ observable is rather stable under perturbative QCD correc-

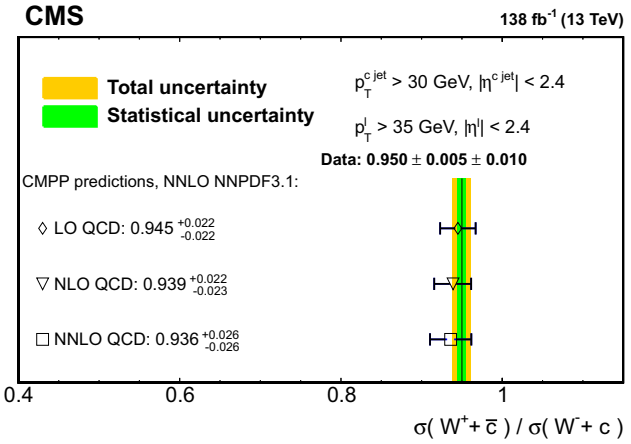

Fig. 12 Comparison of the experimental measurement of $R_c^{\pm}$ with the OS-SS LO, NLO and NNLO QCD predictions. The NNLO QCD NNPDF3.1 PDF set is used for computing all the predictions. CMPP stands for the authors of the calculations [15]. Horizontal error bars indicate the total uncertainty in the predictions

tions, varying by less than 1% from LO to NNLO accuracy. The NLO EW correction does not affect $R_c^{\pm}$, the change being smaller than 0.1%.

The comparison of the predictions with the fiducial inclusive and differential measurements are presented in Figs. 12 and 13. The inclusion of the NNLO QCD correction does not change the good agreement already observed with the predictions at NLO.

9 Summary

The associated production of a W boson with a charm quark (W + c) in proton–proton (pp) collisions at a center-of-mass energy of 13 TeV was studied with a data sample collected by the CMS experiment corresponding to an integrated luminosity of 138 fb^{-1}. The W + c process is selected based on the presence of a high transverse momentum lepton (electron or muon), coming from a W boson decay, and a jet with the signature of a charm hadron decay. Charm hadron decays are identified either by the presence of a muon inside a jet or by reconstructing a secondary decay vertex within the jet. Measurements are combined from the four different channels: electron and muon W boson decay channels, muon and secondary vertex charm identification channels.

Cross section measurements, within a fiducial region defined by the kinematics of the lepton from the W boson decay and the jet originated by the charm quark ($p_{\text{T}}^{\ell} > 35\,\text{GeV}$, $|\eta^{\ell}| < 2.4$, $p_{\text{T}}^{\text{c jet}} > 30\,\text{GeV}$, $|\eta^{\text{c jet}}| < 2.4$), are unfolded to the particle and parton levels. Cross sections are also measured differentially, as functions of $|\eta^{\ell}|$ and p_{T}^{ℓ}. The cross section ratio for the processes $\text{W}^+ + \bar{\text{c}}$ and $\text{W}^- + \text{c}$

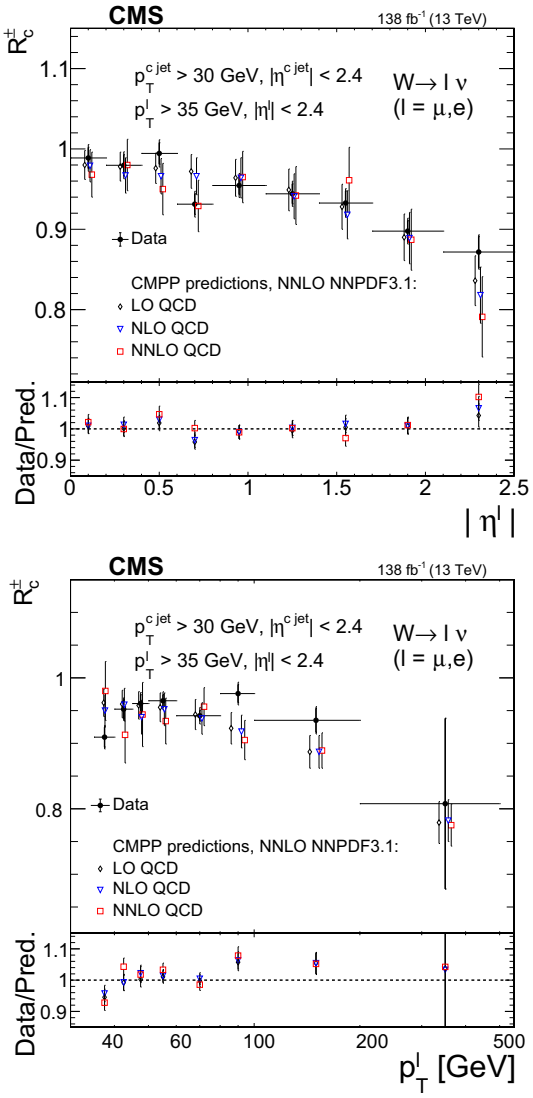

Fig. 13 Comparison of the measured differential cross section ratio $R_c^{\pm}$ as a function of the absolute value of η^{ℓ} (upper) and p_{T}^{ℓ} (lower) with the OS-SS LO, NLO, and NNLO QCD predictions. The NNLO QCD NNPDF3.1 PDF set is used for computing all the predictions. CMPP stands for the authors of the calculations [15]. Error bars on data points include statistical and systematic uncertainties. Symbols showing the theoretical expectations are slightly displaced in the horizontal axis for better visibility. The ratios of data to predictions are shown in the lower panels. The uncertainty in the ratio includes the uncertainties in the data and prediction

is measured as well, achieving the highest precision in this measurement to date.

The measured fiducial $\sigma(\text{W} + \text{c})$ production cross section unfolded to the particle level is:

$$\sigma(\text{pp} \to \text{W} + \text{c})\mathcal{B}(\text{W} \to \ell\nu) = 148.7 \pm 0.4\,(\text{stat}) \pm 5.6\,(\text{syst})\,\text{pb}.$$

The cross section measurement unfolded to the parton level yields:

$$\sigma(\mathrm{pp} \to \mathrm{W} + \mathrm{c})\mathcal{B}(\mathrm{W} \to \ell\nu) = 163.4 \pm 0.5\,(\mathrm{stat}) \pm 6.2\,(\mathrm{syst})\,\mathrm{pb}.$$

The measured $\sigma(\mathrm{W}^+ + \bar{\mathrm{c}})/\sigma(\mathrm{W}^- + \mathrm{c})$ cross section ratio is:

$$\frac{\sigma(\mathrm{pp} \to \mathrm{W}^+ + \bar{\mathrm{c}})}{\sigma(\mathrm{pp} \to \mathrm{W}^- + \mathrm{c})} = 0.950 \pm 0.005\,(\mathrm{stat}) \pm 0.010\,(\mathrm{syst}).$$

The measurements are compared with theoretical predictions. The particle level measurements are compared with the predictions of the MADGRAPH5_aMC@NLO MC generator. The parton level cross section measurements are compared with NLO QCD calculations from the MCFM program using different PDF sets and with recently available NNLO QCD calculations including NLO EW corrections. The predicted fiducial cross section and cross section ratio are consistent with the measurements within uncertainties. The NNLO QCD and NLO EW corrections improve the agreement between the predicted and measured cross sections. Despite the improvement in precision of the cross section ratio measurement compared with previous studies, discrimination between predictions using symmetric or asymmetric strange quark and antiquark PDFs would require a further reduction of experimental and theoretical uncertainties. The theoretical uncertainty is dominated by the PDF uncertainties. The inclusion of the cross section measurements in future PDF fits should improve the modeling of the strange parton distribution function of the proton.

Acknowledgements We congratulate our colleagues in the CERN accelerator departments for the excellent performance of the LHC and thank the technical and administrative staffs at CERN and at other CMS institutes for their contributions to the success of the CMS effort. In addition, we gratefully acknowledge the computing centers and personnel of the Worldwide LHC Computing Grid and other centers for delivering so effectively the computing infrastructure essential to our analyses. Finally, we acknowledge the enduring support for the construction and operation of the LHC, the CMS detector, and the supporting computing infrastructure provided by the following funding agencies: SC (Armenia), BMBWF and FWF (Austria); FNRS and FWO (Belgium); CNPq, CAPES, FAPERJ, FAPERGS, and FAPESP (Brazil); MES and BNSF (Bulgaria); CERN; CAS, MoST, and NSFC (China); MINCIENCIAS (Colombia); MSES and CSF (Croatia); RIF (Cyprus); SENESCYT (Ecuador); MoER, ERC PUT and ERDF (Estonia); Academy of Finland, MEC, and HIP (Finland); CEA and CNRS/IN2P3 (France); BMBF, DFG, and HGF (Germany); GSRI (Greece); NKFIH (Hungary); DAE and DST (India); IPM (Iran); SFI (Ireland); INFN (Italy); MSIP and NRF (Republic of Korea); MES (Latvia); LAS (Lithuania); MOE and UM (Malaysia); BUAP, CINVESTAV, CONACYT, LNS, SEP, and UASLP-FAI (Mexico); MOS (Montenegro); MBIE (New Zealand); PAEC (Pakistan); MES and NSC (Poland); FCT (Portugal); MESTD (Serbia); MCIN/AEI and PCTI (Spain); MOSTR (Sri Lanka); Swiss Funding Agencies (Switzerland); MST (Taipei); MHESI and NSTDA (Thailand); TUBITAK and TENMAK (Turkey); NASU (Ukraine); STFC (United Kingdom); DOE and NSF (USA). Individuals have received support from the Marie-Curie program and the European Research Council and Horizon 2020 Grant, contract Nos. 675440, 683211, 724704, 752730, 758316, 765710, 824093, 884104, and COST Action CA16108 (European Union); the Leventis Foundation; the Alfred P. Sloan Foundation; the Alexander von Humboldt Foundation; the Science Committee, project no. 22rl-037 (Armenia); the Belgian Federal Science Policy Office; the Fonds pour la Formation à la Recherche dans l'Industrie et dans l'Agriculture (FRIA-Belgium); the Agentschap voor Innovatie door Wetenschap en Technologie (IWT-Belgium); the F.R.S.-FNRS and FWO (Belgium) under the "Excellence of Science – EOS" – be.h project n. 30820817; the Beijing Municipal Science & Technology Commission, No. Z191100007219010; the Ministry of Education, Youth and Sports (MEYS) of the Czech Republic; the Shota Rustaveli National Science Foundation, grant FR-22-985 (Georgia); the Deutsche Forschungsgemeinschaft (DFG), under Germany's Excellence Strategy – EXC 2121 "Quantum Universe" – 390833306, and under project number 400140256 - GRK2497, RTG2044, INST 39/963-1 FUGG (bwForCluster NEMO), and 396021762 - TRR 257, and the state of Baden-Württemberg through bwHPC (Germany); the Hellenic Foundation for Research and Innovation (HFRI), Project Number 2288 (Greece); the Hungarian Academy of Sciences, the New National Excellence Program - ÚNKP, the NKFIH research grants K 124845, K 124850, K 128713, K 128786, K 129058, K 131991, K 133046, K 138136, K 143460, K 143477, 2020−2.2.1-ED-2021-00181, and TKP2021-NKTA-64 (Hungary); the Council of Science and Industrial Research, India; the Latvian Council of Science; the Ministry of Education and Science, project no. 2022/WK/14, and the National Science Center, contracts Opus 2021/41/B/ST2/01369 and 2021/43/B/ST2/01552 (Poland); the Fundação para a Ciência e a Tecnologia, grant CEECIND/01334/2018 (Portugal); the National Priorities Research Program by Qatar National Research Fund; MCIN/AEI/10.13039/501100011033, ERDF "a way of making Europe", and the Programa Estatal de Fomento de la Investigación Científica y Técnica de Excelencia María de Maeztu, grant MDM-2017-0765 and Programa Severo Ochoa del Principado de Asturias (Spain); the Chulalongkorn Academic into Its 2nd Century Project Advancement Project, and the National Science, Research and Innovation Fund via the Program Management Unit for Human Resources & Institutional Development, Research and Innovation, grant B05F650021 (Thailand); Isaac Newton Trust, Leverhulme Trust, and STFC grants ST/L002760/1, ST/K004883/1, and ST/T000694/1 (United Kingdom); the Kavli Foundation; the Nvidia Corporation; the SuperMicro Corporation; the Welch Foundation, contract C-1845; and the Weston Havens Foundation (USA).

Data Availability Statement This manuscript has no associated data or the data will not be deposited. [Authors' comment: Release and preservation of data used by the CMS Collaboration as the basis for publications is guided by the CMS policy as stated in https://cms-docdb.cern.ch/cgi-bin/PublicDocDB/RetrieveFile?docid=6032\&filename=CMSDataPolicyV1.2.pdf\&version=2. CMS data preservation, re-use and open access policy].

Declarations

Conflict of interest The authors declare that they have no conflict of interest.

Funded by SCOAP[3].

References

1. U. Baur et al., The charm content of W + 1 jet events as a probe of the strange quark distribution function. Phys. Lett. B **318**, 544 (1993). https://doi.org/10.1016/0370-2693(93)91553-Y. arXiv:hep-ph/9308370
2. S. Catani, D. de Florian, G. Rodrigo, W. Vogelsang, Perturbative generation of a strange-quark asymmetry in the nucleon. Phys. Rev. Lett. **93**, 152003 (2004). https://doi.org/10.1103/PhysRevLett.93.152003. arXiv:hep-ph/0404240
3. H. Lai et al., The strange parton distribution of the nucleon: global analysis and applications. JHEP **04**, 089 (2007). https://doi.org/10.1088/1126-6708/2007/04/089. arXiv:hep-ph/0702268
4. F. Faura et al., The strangest proton? Eur. Phys. J. C **80**, 1168 (2020). https://doi.org/10.1140/epjc/s10052-020-08749-3. arXiv:2009.00014
5. CMS Collaboration, Measurement of associated Z + charm production in proton–proton collisions at $\sqrt{s} = 8$ TeV. Eur. Phys. J. C **78**, 287 (2018). https://doi.org/10.1140/epjc/s10052-018-5752-x. arXiv:1711.02143
6. CMS Collaboration, Search for Higgs boson decay to a charm quark–antiquark pair in proton–proton collisions at $\sqrt{s} = 13$ TeV. Phys. Rev. Lett. **131**, 061801 (2023). https://doi.org/10.1103/PhysRevLett.131.061801. arXiv:2205.05550
7. CMS Collaboration, Measurement of associated W+charm production in pp collisions at $\sqrt{s} = 7$ TeV. JHEP **02**, 013 (2014). https://doi.org/10.1007/JHEP02(2014)013. arXiv:1310.1138
8. CMS Collaboration, Measurements of the production of a W boson in association with a charm quark in proton-proton collisions at $\sqrt{s} = 8$ TeV. Eur. Phys. J. C **82**, 1094 (2022). https://doi.org/10.1140/epjc/s10052-022-10897-7. arXiv:2112.00895
9. CMS Collaboration, Measurement of associated production of a W boson and a charm quark in proton-proton collisions at $\sqrt{s} = 13$ TeV. Eur. Phys. J. C **79**, 269 (2019). https://doi.org/10.1140/epjc/s10052-019-6752-1. arXiv:1811.10021
10. ATLAS Collaboration, Measurement of the production of a W boson in association with a charm quark in pp collisions at $\sqrt{s} = 7$ TeV with the ATLAS detector. JHEP **05**, 068 (2014). https://doi.org/10.1007/JHEP05(2014)068. arXiv:1402.6263
11. ATLAS Collaboration, Measurement of the production of a W boson in association with a charmed hadron in pp collisions at $\sqrt{s} = 13$ TeV with the ATLAS detector (2023). https://doi.org/10.48550/arXiv.2302.00336
12. LHCb Collaboration, Study of W boson production in association with beauty and charm. Phys. Rev. D **92**, 052001 (2015). https://doi.org/10.1103/PhysRevD.92.052001. arXiv:1505.04051
13. W.J. Stirling, E. Vryonidou, Charm production in association with an electroweak gauge boson at the LHC. Phys. Rev. Lett. **109**, 082002 (2012). https://doi.org/10.1103/PhysRevLett.109.082002. arXiv:1203.6781
14. M. Czakon, A. Mitov, M. Pellen, R. Poncelet, NNLO QCD predictions for W + c-jet production at the LHC. JHEP **06**, 100 (2021). https://doi.org/10.1007/JHEP06(2021)100. arXiv:2011.01011
15. M. Czakon, A. Mitov, M. Pellen, R. Poncelet, A detailed investigation of W + c-jet at the LHC. JHEP **02**, 241 (2023). https://doi.org/10.1007/JHEP02(2023)241. arXiv:2212.00467v3
16. J. Campbell, T. Neumann, Precision phenomenology with MCFM. JHEP **12**, 034 (2019). https://doi.org/10.1007/JHEP12(2019)034. arXiv:1909.09117
17. 2023. HEPData record for this analysis (2023). https://doi.org/10.17182/hepdata.141611
18. CMS Collaboration, Track impact parameter resolution in the 2017 dataset with the CMS Phase-1 pixel detector, CMS Detector Performance Note CMS-DP-2020-032 (2020)
19. W. Adam et al., The CMS Phase-1 pixel detector upgrade. JINST **16**, P02027 (2021). https://doi.org/10.1088/1748-0221/16/02/p02027. arXiv:2012.14304
20. CMS Collaboration, Performance of b tagging algorithms in proton–proton collisions at 13 TeV with Phase-1 CMS detector, CMS Detector Performance Note CMS-DP-2018-033 (2018)
21. CMS Collaboration, The CMS experiment at the CERN LHC. JINST **3**, S08004 (2008). https://doi.org/10.1088/1748-0221/3/08/S08004
22. CMS Collaboration, Performance of the CMS Level-1 trigger in proton–proton collisions at $\sqrt{s} = 13$ TeV. JINST **15**, P10017 (2020). https://doi.org/10.1088/1748-0221/15/10/P10017. arXiv:2006.10165
23. CMS Collaboration, The CMS trigger system. JINST **12**, P01020 (2017). https://doi.org/10.1088/1748-0221/12/01/P01020. arXiv:1609.02366
24. J. Alwall et al., The automated computation of tree-level and next-to-leading order differential cross sections, and their matching to parton shower simulations. JHEP **07**, 079 (2014). https://doi.org/10.1007/JHEP07(2014)079. arXiv:1405.0301
25. S. Alioli, P. Nason, C. Oleari, E. Re, A general framework for implementing NLO calculations in shower Monte Carlo programs: the POWHEG BOX. JHEP **06**, 043 (2010). https://doi.org/10.1007/JHEP06(2010)043. arXiv:1002.2581
26. Y. Li, F. Petriello, Combining QCD and electroweak corrections to dilepton production in the framework of the FEWZ simulation code. Phys. Rev. D **86**, 094034 (2012). https://doi.org/10.1103/PhysRevD.86.094034. arXiv:1208.5967
27. M. Czakon, A. Mitov, Top++: a program for the calculation of the top-pair cross-section at hadron colliders. Comput. Phys. Commun. **185**, 2930 (2014). https://doi.org/10.1016/j.cpc.2014.06.021. arXiv:1112.5675
28. T. Sjöstrand et al., An introduction to PYTHIA 8.2. Comput. Phys. Commun. **191**, 159 (2015). https://doi.org/10.1016/j.cpc.2015.01.024. arXiv:1410.3012
29. NNPDF Collaboration, Parton distributions for the LHC Run II. JHEP **04**, 040 (2015). https://doi.org/10.1007/JHEP04(2015)040. arXiv:1410.8849
30. NNPDF Collaboration, Parton distributions from high-precision collider data. Eur. Phys. J. C **77**, 663 (2017). https://doi.org/10.1140/epjc/s10052-017-5199-5. arXiv:1706.00428
31. P. Skands, S. Carrazza, J. Rojo, Tuning PYTHIA 8.1: the Monash 2013 Tune. Eur. Phys. J. C **74**, 3024 (2014). https://doi.org/10.1140/epjc/s10052-014-3024-y. arXiv:1404.5630
32. CMS Collaboration, Event generator tunes obtained from underlying event and multiparton scattering measurements. Eur. Phys. J. C **76**, 155 (2016). https://doi.org/10.1140/epjc/s10052-016-3988-x. arXiv:1512.00815
33. CMS Collaboration, Extraction and validation of a new set of CMS PYTHIA8 tunes from underlying-event measurements. Eur. Phys. J. C **80**, 4 (2020). https://doi.org/10.1140/epjc/s10052-019-7499-4. arXiv:1903.12179
34. R. Frederix, S. Frixione, Merging meets matching in MC@NLO. JHEP **12**, 061 (2012). https://doi.org/10.1007/JHEP12(2012)061. arXiv:1209.6215
35. M. Lisovyi, A. Verbytskyi, O. Zenaiev, Combined analysis of charm-quark fragmentation-fraction measurements. Eur. Phys. J. C

76, 397 (2016). https://doi.org/10.1140/epjc/s10052-016-4246-y. arXiv:1509.01061
36. R.L. Workman and others (Particle Data Group), Review of Particle Physics, PTEP **2022** (2022) 083C01. https://doi.org/10.1093/ptep/ptac097
37. Geant4 Collaboration, Geant4—a simulation toolkit. Nucl. Instrum. Methods A **506**, 250 (2003). https://doi.org/10.1016/S0168-9002(03)01368-8
38. CMS Collaboration, Particle-flow reconstruction and global event description with the CMS detector. JINST **12**, P10003 (2017). https://doi.org/10.1088/1748-0221/12/10/P10003. arXiv:1706.04965
39. CMS Collaboration, Technical proposal for the phase-II upgrade of the Compact Muon Solenoid. CMS Technical Proposal, (2015). CERN-LHCC-2015-010, CMS-TDR-15-02. http://cds.cern.ch/record/2020886
40. CMS Collaboration, Electron and photon reconstruction and identification with the CMS experiment at the CERN LHC. JINST **16**, P05014 (2021). https://doi.org/10.1088/1748-0221/16/05/P05014. arXiv:2012.06888
41. CMS Collaboration, ECAL 2016 refined calibration and run 2 summary plots. CMS Detector Performance Note, (2020). CMS-DP-2020-021. https://cds.cern.ch/record/2717925
42. CMS Collaboration, Performance of the CMS muon detector and muon reconstruction with proton-proton collisions at $\sqrt{s} = 13$ TeV. JINST **13**, P06015 (2018). https://doi.org/10.1088/1748-0221/13/06/P06015. arXiv:1804.04528
43. M. Cacciari, G.P. Salam, G. Soyez, The anti-k_T jet clustering algorithm. JHEP **04**, 063 (2008). https://doi.org/10.1088/1126-6708/2008/04/063. arXiv:0802.1189
44. M. Cacciari, G.P. Salam, G. Soyez, FastJet user manual. Eur. Phys. J. C **72**, 1896 (2012). https://doi.org/10.1140/epjc/s10052-012-1896-2. arXiv:1111.6097
45. CMS Collaboration, Jet energy scale and resolution in the CMS experiment in pp collisions at 8 TeV. JINST **12**, P02014 (2017). https://doi.org/10.1088/1748-0221/12/02/P02014. arXiv:1607.03663
46. CMS Collaboration, Performance of missing transverse momentum reconstruction in proton-proton collisions at $\sqrt{s} = 13$ TeV using the CMS detector. JINST **14**, P07004 (2019). https://doi.org/10.1088/1748-0221/14/07/P07004. arXiv:1903.06078
47. CMS Collaboration, Measurement of the inclusive W and Z production cross sections in pp collisions at $\sqrt{s} = 7$ TeV with the CMS experiment. JHEP **10**, 132 (2011). https://doi.org/10.1007/JHEP10(2011)132. arXiv:1107.4789
48. M. Cacciari, G.P. Salam, Pileup subtraction using jet areas. Phys. Lett. B **659**, 119 (2008). https://doi.org/10.1016/j.physletb.2007.09.077. arXiv:0707.1378
49. CMS Collaboration, Identification of heavy-flavour jets with the CMS detector in pp collisions at 13 TeV. JINST **13**, P05011 (2018). https://doi.org/10.1088/1748-0221/13/05/P05011. arXiv:1712.07158
50. CMS Collaboration, Identification of b-quark jets with the CMS experiment. JINST **8**, P04013 (2013). https://doi.org/10.1088/1748-0221/8/04/P04013. arXiv:1211.4462
51. CMS Collaboration, Measurement of $b\bar{b}$ angular correlations based on secondary vertex reconstruction at $\sqrt{s} = 7$ TeV. JHEP **03**, 136 (2011). https://doi.org/10.1007/JHEP03(2011)136. arXiv:1102.3194
52. CMS Collaboration, Measurement of the cross section and angular correlations for associated production of a Z boson with b hadrons in pp collisions at $\sqrt{s} = 7$ TeV. JHEP **12**, 039 (2013). https://doi.org/10.1007/JHEP12(2013)039. arXiv:1310.1349
53. W. Waltenberger, R. Frühwirth, P. Vanlaer, Adaptive vertex fitting. J. Phys. G **34**, N343 (2007). https://doi.org/10.1088/0954-3899/34/12/N01
54. A. Ali, F. Barreiro, The final states $\ell^{\pm} K^{\pm} K^{\pm}$ X in jets as signatures of B_s^0-$\bar{B}_s^0$ mixings. Z. Phys. C **30**, 635 (1986). https://doi.org/10.1007/BF01571814
55. M. Gronau, A. Nippe, J.L. Rosner, Method for flavor tagging in neutral B meson decays. Phys. Rev. D **47**, 1988 (1993). https://doi.org/10.1103/PhysRevD.47.1988. arXiv:hep-ph/9211311
56. LHCb Collaboration, Identification of beauty and charm quark jets at LHCb. JINST **10**, P06013 (2015). https://doi.org/10.1088/1748-0221/10/06/P06013. arXiv:1504.07670
57. CMS Collaboration, Measurement of the inelastic proton-proton cross section at $\sqrt{s} = 13$ TeV. JHEP **07**, 161 (2018). https://doi.org/10.1007/JHEP07(2018)161. arXiv:1802.02613
58. CMS Collaboration, Precision luminosity measurement in proton-proton collisions at $\sqrt{s} = 13$ TeV in 2015 and 2016 at CMS. Eur. Phys. J. C **81**, 800 (2021). https://doi.org/10.1140/epjc/s10052-021-09538-2. arXiv:2104.01927
59. CMS Collaboration, CMS luminosity measurement for the 2017 data-taking period at $\sqrt{s} = 13$ TeV. CMS Physics Analysis Summary (2018). CMS-PAS-LUM-17-004. https://cds.cern.ch/record/2621960/
60. CMS Collaboration, CMS luminosity measurement for the 2018 data-taking period at $\sqrt{s} = 13$ TeV. CMS Physics Analysis Summary (2019). CMS-PAS-LUM-18-002. https://cds.cern.ch/record/2676164/
61. J. Butterworth et al., PDF4LHC recommendations for LHC run II. J. Phys. G **43**, 023001 (2016). https://doi.org/10.1088/0954-3899/43/2/023001. arXiv:1510.03865
62. L. Lyons, D. Gibaut, P. Clifford, How to combine correlated estimates of a single physical quantity. Nucl. Instrum. Methods A **270**, 110 (1988). https://doi.org/10.1016/0168-9002(88)90018-6
63. S. Bailey et al., Parton distributions from LHC, HERA, Tevatron and fixed target data: MSHT20 PDFs. Eur. Phys. J. C **81**, 341 (2021). https://doi.org/10.1140/epjc/s10052-021-09057-0. arXiv:2012.04684
64. T.-J. Hou et al., New CTEQ global analysis of quantum chromodynamics with high-precision data from the LHC. Phys. Rev. D **103**, 014013 (2021). https://doi.org/10.1103/PhysRevD.103.014013. arXiv:1912.10053
65. S. Alekhin, J. Blümlein, S. Moch, NLO PDFs from the ABMP16 fit. Eur. Phys. J. C **78**, 477 (2018). https://doi.org/10.1140/epjc/s10052-018-5947-1. arXiv:1803.07537
66. A. Buckley et al., LHAPDF6: parton density access in the LHC precision era. Eur. Phys. J. C **75**, 132 (2015). https://doi.org/10.1140/epjc/s10052-015-3318-8. arXiv:1412.7420
67. ATLAS Collaboration, Precision measurement and interpretation of inclusive W^+, W^- and Z/γ^* production cross sections with the ATLAS detector. Eur. Phys. J. C **77**, 367 (2017). https://doi.org/10.1140/epjc/s10052-017-4911-9. arXiv:1612.03016
68. M. Czakon, A. Mitov, R. Poncelet, Infrared-safe flavoured anti-k_T jets. JHEP **04**, 138 (2023). https://doi.org/10.1007/JHEP04(2023)138. arXiv:2205.11879
69. S. Carrazza, S. Forte, Z. Kassabov, J. Rojo, Specialized minimal PDFs for optimized LHC calculations. Eur. Phys. J. C **76**, 205 (2016). https://doi.org/10.1140/epjc/s10052-016-4042-8. arXiv:1602.00005

CMS Collaboration

Yerevan Physics Institute, Yerevan, Armenia
A. Tumasyan[1]

Institut für Hochenergiephysik, Vienna, Austria
W. Adam, J. W. Andrejkovic, T. Bergauer, S. Chatterjee, K. Damanakis, M. Dragicevic, A. Escalante Del Valle, P. S. Hussain, M. Jeitler[2], N. Krammer, L. Lechner, D. Liko, I. Mikulec, P. Paulitsch, F. M. Pitters, J. Schieck[2], R. Schöfbeck, D. Schwarz, M. Sonawane, S. Templ, W. Waltenberger, C.-E. Wulz[2]

Universiteit Antwerpen, Antwerpen, Belgium
M. R. Darwish[3], T. Janssen, T. Kello[4], H. Rejeb Sfar, P. Van Mechelen

Vrije Universiteit Brussel, Brussel, Belgium
E. S. Bols, J. D'Hondt, A. De Moor, M. Delcourt, H. El Faham, S. Lowette, S. Moortgat, A. Morton, D. Müller, A. R. Sahasransu, S. Tavernier, W. Van Doninck, D. Vannerom

Université Libre de Bruxelles, Bruxelles, Belgium
B. Clerbaux, G. De Lentdecker, L. Favart, D. Hohov, J. Jaramillo, K. Lee, M. Mahdavikhorrami, I. Makarenko, A. Malara, S. Paredes, L. Pétré, N. Postiau, L. Thomas, M. Vanden Bemden, C. Vander Velde, P. Vanlaer

Ghent University, Ghent, Belgium
D. Dobur, J. Knolle, L. Lambrecht, G. Mestdach, C. Rendón, A. Samalan, K. Skovpen, M. Tytgat, N. Van Den Bossche, B. Vermassen, L. Wezenbeek

Université Catholique de Louvain, Louvain-la-Neuve, Belgium
A. Benecke, G. Bruno, F. Bury, C. Caputo, P. David, C. Delaere, I. S. Donertas, A. Giammanco, K. Jaffel, Sa. Jain, V. Lemaitre, K. Mondal, A. Taliercio, T. T. Tran, P. Vischia, S. Wertz

Centro Brasileiro de Pesquisas Fisicas, Rio de Janeiro, Brazil
G. A. Alves, E. Coelho, C. Hensel, A. Moraes, P. Rebello Teles

Universidade do Estado do Rio de Janeiro, Rio de Janeiro, Brazil
W. L. Aldá Júnior, M. Alves Gallo Pereira, M. Barroso Ferreira Filho, H. Brandao Malbouisson, W. Carvalho, J. Chinellato[5], E. M. Da Costa, G. G. Da Silveira[6], D. De Jesus Damiao, V. Dos Santos Sousa, S. Fonseca De Souza, J. Martins[7], C. Mora Herrera, K. Mota Amarilo, L. Mundim, H. Nogima, A. Santoro, S. M. Silva Do Amaral, A. Sznajder, M. Thiel, A. Vilela Pereira

Universidade Estadual Paulista, Universidade Federal do ABC, São Paulo, Brazil
C. A. Bernardes[6], L. Calligaris, T. R. Fernandez Perez Tomei, E. M. Gregores, P. G. Mercadante, S. F. Novaes, Sandra S. Padula

Institute for Nuclear Research and Nuclear Energy, Bulgarian Academy of Sciences, Sofia, Bulgaria
A. Aleksandrov, G. Antchev, R. Hadjiiska, P. Iaydjiev, M. Misheva, M. Rodozov, M. Shopova, G. Sultanov

University of Sofia, Sofia, Bulgaria
A. Dimitrov, T. Ivanov, L. Litov, B. Pavlov, P. Petkov, A. Petrov, E. Shumka

Instituto De Alta Investigación, Universidad de Tarapacá, Casilla 7 D, Arica, Chile
S. Thakur

Beihang University, Beijing, China
T. Cheng, T. Javaid[8], M. Mittal, L. Yuan

Department of Physics, Tsinghua University, Beijing, China
M. Ahmad, G. Bauer[9], Z. Hu, S. Lezki, K. Yi[9,10]

Institute of High Energy Physics, Beijing, China
G. M. Chen[8], H. S. Chen[8], M. Chen[8], F. Iemmi, C. H. Jiang, A. Kapoor, H. Liao, Z.-A. Liu[11], V. Milosevic, F. Monti, R. Sharma, J. Tao, J. Thomas-Wilsker, J. Wang, H. Zhang, J. Zhao

State Key Laboratory of Nuclear Physics and Technology, Peking University, Beijing, China
A. Agapitos, Y. An, Y. Ban, A. Levin, C. Li, Q. Li, X. Lyu, Y. Mao, S. J. Qian, X. Sun, D. Wang, J. Xiao, H. Yang

Sun Yat-Sen University, Guangzhou, China
M. Lu, Z. You

University of Science and Technology of China, Hefei, China
N. Lu

Institute of Modern Physics and Key Laboratory of Nuclear Physics and Ion-beam Application (MOE), Fudan University, Shanghai, China
X. Gao[4], D. Leggat, H. Okawa, Y. Zhang

Zhejiang University, Hangzhou, Zhejiang, China
Z. Lin, C. Lu, M. Xiao

Universidad de Los Andes, Bogota, Colombia
C. Avila, D. A. Barbosa Trujillo, A. Cabrera, C. Florez, J. Fraga

Universidad de Antioquia, Medellin, Colombia
J. Mejia Guisao, F. Ramirez, M. Rodriguez, J. D. Ruiz Alvarez

Faculty of Electrical Engineering, Mechanical Engineering and Naval Architecture, University of Split, Split, Croatia
D. Giljanovic, N. Godinovic, D. Lelas, I. Puljak

Faculty of Science, University of Split, Split, Croatia
Z. Antunovic, M. Kovac, T. Sculac

Institute Rudjer Boskovic, Zagreb, Croatia
V. Brigljevic, B. K. Chitroda, D. Ferencek, S. Mishra, M. Roguljic, A. Starodumov[12], T. Susa

University of Cyprus, Nicosia, Cyprus
A. Attikis, K. Christoforou, M. Kolosova, S. Konstantinou, J. Mousa, C. Nicolaou, F. Ptochos, P. A. Razis, H. Rykaczewski, H. Saka, A. Stepennov

Charles University, Prague, Czech Republic
M. Finger, M. Finger Jr., A. Kveton

Escuela Politecnica Nacional, Quito, Ecuador
E. Ayala

Universidad San Francisco de Quito, Quito, Ecuador
E. Carrera Jarrin

Academy of Scientific Research and Technology of the Arab Republic of Egypt, Egyptian Network of High Energy Physics, Cairo, Egypt
S. Elgammal[13], A. Ellithi Kamel[14]

Center for High Energy Physics (CHEP-FU), Fayoum University, El-Fayoum, Egypt
M. A. Mahmoud, Y. Mohammed

National Institute of Chemical Physics and Biophysics, Tallinn, Estonia
S. Bhowmik, R. K. Dewanjee, K. Ehataht, M. Kadastik, T. Lange, S. Nandan, C. Nielsen, J. Pata, M. Raidal, L. Tani, C. Veelken

Department of Physics, University of Helsinki, Helsinki, Finland
P. Eerola, H. Kirschenmann, K. Osterberg, M. Voutilainen

Helsinki Institute of Physics, Helsinki, Finland
S. Bharthuar, E. Brücken, F. Garcia, J. Havukainen, M. S. Kim, R. Kinnunen, T. Lampén, K. Lassila-Perini, S. Lehti, T. Lindén, M. Lotti, L. Martikainen, M. Myllymäki, J. Ott, M.m. Rantanen, H. Siikonen, E. Tuominen, J. Tuominiemi

Lappeenranta-Lahti University of Technology, Lappeenranta, Finland
P. Luukka, H. Petrow, T. Tuuva

IRFU, CEA, Université Paris-Saclay, Gif-sur-Yvette, France
C. Amendola, M. Besancon, F. Couderc, M. Dejardin, D. Denegri, J. L. Faure, F. Ferri, S. Ganjour, P. Gras, G. Hamel de Monchenault, V. Lohezic, J. Malcles, J. Rander, A. Rosowsky, M.Ö. Sahin, A. Savoy-Navarro[15], P. Simkina, M. Titov

Laboratoire Leprince-Ringuet, CNRS/IN2P3, Ecole Polytechnique, Institut Polytechnique de Paris, Palaiseau, France
C. Baldenegro Barrera, F. Beaudette, A. Buchot Perraguin, P. Busson, A. Cappati, C. Charlot, F. Damas, O. Davignon, B. Diab, G. Falmagne, B. A. Fontana Santos Alves, S. Ghosh, R. Granier de Cassagnac, A. Hakimi, B. Harikrishnan, G. Liu, J. Motta, M. Nguyen, C. Ochando, L. Portales, R. Salerno, U. Sarkar, J. B. Sauvan, Y. Sirois, A. Tarabini, E. Vernazza, A. Zabi, A. Zghiche

Université de Strasbourg, CNRS, IPHC UMR 7178, Strasbourg, France
J.-L. Agram[16], J. Andrea, D. Apparu, D. Bloch, G. Bourgatte, J.-M. Brom, E. C. Chabert, C. Collard, D. Darej, U. Goerlach, C. Grimault, A.-C. Le Bihan, P. Van Hove

Institut de Physique des 2 Infinis de Lyon (IP2I), Villeurbanne, France
S. Beauceron, B. Blancon, G. Boudoul, A. Carle, N. Chanon, J. Choi, D. Contardo, P. Depasse, C. Dozen[17], H. El Mamouni, J. Fay, S. Gascon, M. Gouzevitch, G. Grenier, B. Ille, I. B. Laktineh, M. Lethuillier, L. Mirabito, S. Perries, L. Torterotot, M. Vander Donckt, P. Verdier, S. Viret

Georgian Technical University, Tbilisi, Georgia
I. Bagaturia[18], I. Lomidze, Z. Tsamalaidze[12]

I. Physikalisches Institut, RWTH Aachen University, Aachen, Germany
V. Botta, L. Feld, K. Klein, M. Lipinski, D. Meuser, A. Pauls, N. Röwert, M. Teroerde

III. Physikalisches Institut A, RWTH Aachen University, Aachen, Germany
S. Diekmann, A. Dodonova, N. Eich, D. Eliseev, M. Erdmann, P. Fackeldey, D. Fasanella, B. Fischer, T. Hebbeker, K. Hoepfner, F. Ivone, M.y. Lee, L. Mastrolorenzo, M. Merschmeyer, A. Meyer, S. Mondal, S. Mukherjee, D. Noll, A. Novak, F. Nowotny, A. Pozdnyakov, Y. Rath, W. Redjeb, H. Reithler, A. Schmidt, S. C. Schuler, A. Sharma, A. Stein, F. Torres Da Silva De Araujo[19], L. Vigilante, S. Wiedenbeck, S. Zaleski

III. Physikalisches Institut B, RWTH Aachen University, Aachen, Germany
C. Dziwok, G. Flügge, W. Haj Ahmad[20], O. Hlushchenko, T. Kress, A. Nowack, O. Pooth, A. Stahl, T. Ziemons, A. Zotz

Deutsches Elektronen-Synchrotron, Hamburg, Germany
H. Aarup Petersen, M. Aldaya Martin, P. Asmuss, S. Baxter, M. Bayatmakou, O. Behnke, A. Bermúdez Martínez, S. Bhattacharya, A. A. Bin Anuar, F. Blekman[21], K. Borras[22], D. Brunner, A. Campbell, A. Cardini, C. Cheng, F. Colombina, S. Consuegra Rodríguez, G. Correia Silva, M. De Silva, L. Didukh, G. Eckerlin, D. Eckstein, L. I. Estevez Banos, O. Filatov, E. Gallo[21], A. Geiser, A. Giraldi, G. Greau, A. Grohsjean, V. Guglielmi, M. Guthoff, A. Jafari[23], N. Z. Jomhari, B. Kaech, M. Kasemann, H. Kaveh, C. Kleinwort, R. Kogler, M. Komm, D. Krücker, W. Lange, D. Leyva Pernia, K. Lipka[24], W. Lohmann[25], R. Mankel, I.-A. Melzer-Pellmann, M. Mendizabal Morentin, J. Metwally, A. B. Meyer, G. Milella, M. Mormile, A. Mussgiller, A. Nürnberg, Y. Otarid, D. Pérez Adán, A. Raspereza, B. Ribeiro Lopes, J. Rübenach, A. Saggio, A. Saibel, M. Savitskyi, M. Scham[22,26], V. Scheurer, S. Schnake[22], P. Schütze, C. Schwanenberger[21], M. Shchedrolosiev, R. E. Sosa Ricardo, D. Stafford,

N. Tonon[†], M. Van De Klundert, F. Vazzoler, A. Ventura Barroso, R. Walsh, D. Walter, Q. Wang, Y. Wen, K. Wichmann, L. Wiens[22], C. Wissing, S. Wuchterl, Y. Yang, A. Zimermmane Castro Santos

University of Hamburg, Hamburg, Germany
A. Albrecht, S. Albrecht, M. Antonello, S. Bein, L. Benato, M. Bonanomi, P. Connor, K. De Leo, M. Eich, K. El Morabit, F. Feindt, A. Fröhlich, C. Garbers, E. Garutti, M. Hajheidari, J. Haller, A. Hinzmann, H. R. Jabusch, G. Kasieczka, P. Keicher, R. Klanner, W. Korcari, T. Kramer, V. Kutzner, F. Labe, J. Lange, A. Lobanov, C. Matthies, A. Mehta, L. Moureaux, M. Mrowietz, A. Nigamova, Y. Nissan, A. Paasch, K. J. Pena Rodriguez, T. Quadfasel, M. Rieger, O. Rieger, D. Savoiu, J. Schindler, P. Schleper, M. Schröder, J. Schwandt, M. Sommerhalder, H. Stadie, G. Steinbrück, A. Tews, M. Wolf

Karlsruher Institut fuer Technologie, Karlsruhe, Germany
S. Brommer, M. Burkart, E. Butz, R. Caspart, T. Chwalek, A. Dierlamm, A. Droll, N. Faltermann, M. Giffels, J. O. Gosewisch, A. Gottmann, F. Hartmann[27], M. Horzela, U. Husemann, M. Klute, R. Koppenhöfer, M. Link, A. Lintuluoto, S. Maier, S. Mitra, Th. Müller, M. Neukum, M. Oh, G. Quast, K. Rabbertz, J. Rauser, M. Schnepf, I. Shvetsov, H. J. Simonis, N. Trevisani, R. Ulrich, J. van der Linden, R. F. Von Cube, M. Wassmer, S. Wieland, R. Wolf, S. Wozniewski, S. Wunsch, X. Zuo

Institute of Nuclear and Particle Physics (INPP), NCSR Demokritos, Agia Paraskevi, Greece
G. Anagnostou, P. Assiouras, G. Daskalakis, A. Kyriakis, A. Stakia

National and Kapodistrian University of Athens, Athens, Greece
M. Diamantopoulou, D. Karasavvas, P. Kontaxakis, A. Manousakis-Katsikakis, A. Panagiotou, I. Papavergou, N. Saoulidou, K. Theofilatos, E. Tziaferi, K. Vellidis, I. Zisopoulos

National Technical University of Athens, Athens, Greece
G. Bakas, T. Chatzistavrou, K. Kousouris, I. Papakrivopoulos, G. Tsipolitis, A. Zacharopoulou

University of Ioánnina, Ioannina, Greece
K. Adamidis, I. Bestintzanos, I. Evangelou, C. Foudas, P. Gianneios, C. Kamtsikis, P. Katsoulis, P. Kokkas, P. G. Kosmoglou Kioseoglou, N. Manthos, I. Papadopoulos, J. Strologas

MTA-ELTE Lendület CMS Particle and Nuclear Physics Group, Eötvös Loránd University, Budapest, Hungary
M. Csanád, K. Farkas, M. M. A. Gadallah[28], S. Lökös[29], P. Major, K. Mandal, G. Pásztor, A. J. Rádl[30], O. Surányi, G. I. Veres

Wigner Research Centre for Physics, Budapest, Hungary
M. Bartók[31], G. Bencze, C. Hajdu, D. Horvath[32,33], F. Sikler, V. Veszpremi

Institute of Nuclear Research ATOMKI, Debrecen, Hungary
N. Beni, S. Czellar, J. Karancsi[31], J. Molnar, Z. Szillasi, D. Teyssier

Institute of Physics, University of Debrecen, Debrecen, Hungary
P. Raics, B. Ujvari[34]

Karoly Robert Campus, MATE Institute of Technology, Gyongyos, Hungary
T. Csorgo[30], F. Nemes[30], T. Novak

Panjab University, Chandigarh, India
J. Babbar, S. Bansal, S. B. Beri, V. Bhatnagar, G. Chaudhary, S. Chauhan, N. Dhingra[35], R. Gupta, A. Kaur, A. Kaur, H. Kaur, M. Kaur, S. Kumar, P. Kumari, M. Meena, K. Sandeep, T. Sheokand, J. B. Singh[36], A. Singla, A. K. Virdi

University of Delhi, Delhi, India
A. Ahmed, A. Bhardwaj, A. Chhetri, B. C. Choudhary, A. Kumar, M. Naimuddin, K. Ranjan, S. Saumya

Saha Institute of Nuclear Physics, HBNI, Kolkata, India
S. Baradia, S. Barman[37], S. Bhattacharya, D. Bhowmik, S. Dutta, S. Dutta, B. Gomber[38], M. Maity[37], P. Palit, G. Saha, B. Sahu, S. Sarkar

Indian Institute of Technology Madras, Madras, India
P. K. Behera, S. C. Behera, S. Chatterjee, P. Kalbhor, J. R. Komaragiri[39], D. Kumar[39], A. Muhammad, L. Panwar[39], R. Pradhan, P. R. Pujahari, A. Sharma, A. K. Sikdar, P. C. Tiwari[39], S. Verma

Bhabha Atomic Research Centre, Mumbai, India
K. Naskar[40]

Tata Institute of Fundamental Research-A, Mumbai, India
T. Aziz, I. Das, S. Dugad, M. Kumar, G. B. Mohanty, P. Suryadevara

Tata Institute of Fundamental Research-B, Mumbai, India
S. Banerjee, R. Chudasama, M. Guchait, S. Karmakar, S. Kumar, G. Majumder, K. Mazumdar, S. Mukherjee, A. Thachayath

National Institute of Science Education and Research, An OCC of Homi Bhabha National Institute, Bhubaneswar, Odisha, India
S. Bahinipati[41], A. K. Das, C. Kar, P. Mal, T. Mishra, V. K. Muraleedharan Nair Bindhu[42], A. Nayak[42], P. Saha, S. K. Swain, D. Vats[42]

Indian Institute of Science Education and Research (IISER), Pune, India
A. Alpana, S. Dube, B. Kansal, A. Laha, S. Pandey, A. Rastogi, S. Sharma

Isfahan University of Technology, Isfahan, Iran
H. Bakhshiansohi[43,44], E. Khazaie[44], M. Zeinali[45]

Institute for Research in Fundamental Sciences (IPM), Tehran, Iran
S. Chenarani[46], S. M. Etesami, M. Khakzad, M. Mohammadi Najafabadi

University College Dublin, Dublin, Ireland
M. Grunewald

INFN Sezione di Bari[a], Università di Bari[b], Politecnico di Bari[c], Bari, Italy
M. Abbrescia[a,b], R. Aly[a,b,47], C. Aruta[a,b], A. Colaleo[a], D. Creanza[a,c], N. De Filippis[a,c], M. De Palma[a,b], A. Di Florio[a,b], W. Elmetenawee[a,b], F. Errico[a,b], L. Fiore[a], G. Iaselli[a,c], G. Maggi[a,c], M. Maggi[a], I. Margjeka[a,b], V. Mastrapasqua[a,b], S. My[a,b], S. Nuzzo[a,b], A. Pellecchia[a,b], A. Pompili[a,b], G. Pugliese[a,c], R. Radogna[a], D. Ramos[a], A. Ranieri[a], G. Selvaggi[a,b], L. Silvestris[a], F. M. Simone[a,b], Ü. Sözbilir[a], A. Stamerra[a], R. Venditti[a], P. Verwilligen[a]

INFN Sezione di Bologna[a], Università di Bologna[b], Bologna, Italy
G. Abbiendi[a], C. Battilana[a,b], D. Bonacorsi[a,b], L. Borgonovi[a], R. Campanini[a,b], P. Capiluppi[a,b], A. Castro[a,b], F. R. Cavallo[a], C. Ciocca[a], M. Cuffiani[a,b], G. M. Dallavalle[a], T. Diotalevi[a,b], F. Fabbri[a], A. Fanfani[a,b], P. Giacomelli[a], L. Giommi[a,b], C. Grandi[a], L. Guiducci[a,b], S. Lo Meo[a,48], L. Lunerti[a,b], S. Marcellini[a], G. Masetti[a], F. L. Navarria[a,b], A. Perrotta[a], F. Primavera[a,b], A. M. Rossi[a,b], T. Rovelli[a,b], G. P. Siroli[a,b]

INFN Sezione di Catania[a], Università di Catania[b], Catania, Italy
S. Costa[a,b,49], A. Di Mattia[a], R. Potenza[a,b], A. Tricomi[a,b,49], C. Tuve[a,b]

INFN Sezione di Firenze[a], Università di Firenze[b], Firenze, Italy
G. Barbagli[a], G. Bardelli[a,b], B. Camaiani[a,b], A. Cassese[a], R. Ceccarelli[a,b], V. Ciulli[a,b], C. Civinini[a], R. D'Alessandro[a,b], E. Focardi[a,b], G. Latino[a,b], P. Lenzi[a,b], M. Lizzo[a,b], M. Meschini[a], S. Paoletti[a], R. Seidita[a,b], G. Sguazzoni[a], L. Viliani[a]

INFN Laboratori Nazionali di Frascati, Frascati, Italy
L. Benussi, S. Bianco, S. Meola[50], D. Piccolo

INFN Sezione di Genova[a], Università di Genova[b], Genoa, Italy
M. Bozzo[a,b], P. Chatagnon[a], F. Ferro[a], E. Robutti[a], S. Tosi[a,b]

INFN Sezione di Milano-Bicocca[a], Università di Milano-Bicocca[b], Milan, Italy
A. Benaglia[a], G. Boldrini[a], F. Brivio[a,b], F. Cetorelli[a,b], F. De Guio[a,b], M. E. Dinardo[a,b], P. Dini[a], S. Gennai[a], A. Ghezzi[a,b], P. Govoni[a,b], L. Guzzi[a,b], M. T. Lucchini[a,b], M. Malberti[a], S. Malvezzi[a], A. Massironi[a], D. Menasce[a], L. Moroni[a], M. Paganoni[a,b], D. Pedrini[a], B. S. Pinolini[a], S. Ragazzi[a,b], N. Redaelli[a], T. Tabarelli de Fatis[a,b], D. Zuolo[a,b]

INFN Sezione di Napoli[a], Università di Napoli 'Federico II'[b], Napoli, Italy; Università della Basilicata[c], Potenza, Italy, Università G. Marconi[d], Rome, Italy
S. Buontempo[a], F. Carnevali[a,b], N. Cavallo[a,c], A. De Iorio[a,b], F. Fabozzi[a,c], A. O. M. Iorio[a,b], L. Lista[a,b,51], P. Paolucci[a,27], B. Rossi[a], C. Sciacca[a,b]

INFN Sezione di Padova[a], Università di Padova[b], Padova, Italy; Università di Trento[c], Trento, Italy
P. Azzi[a], N. Bacchetta[a,52], D. Bisello[a,b], P. Bortignon[a], A. Bragagnolo[a,b], R. Carlin[a,b], P. Checchia[a], T. Dorigo[a], U. Gasparini[a,b], G. Grosso[a], M. Gulmini[a,53], L. Layer[a,54], E. Lusiani[a], M. Margoni[a,b], G. Maron[a,53], J. Pazzini[a,b], P. Ronchese[a,b], R. Rossin[a,b], F. Simonetto[a,b], G. Strong[a], M. Tosi[a,b], H. Yarar[a,b], M. Zanetti[a,b], P. Zotto[a,b], A. Zucchetta[a,b], G. Zumerle[a,b]

INFN Sezione di Pavia[a], Università di Pavia[b], Pavia, Italy
S. Abu Zeid[a,55], C. Aimè[a,b], A. Braghieri[a], S. Calzaferri[a,b], D. Fiorina[a,b], P. Montagna[a,b], V. Re[a], C. Riccardi[a,b], P. Salvini[a], I. Vai[a], P. Vitulo[a,b]

INFN Sezione di Perugia[a], Università di Perugia[b], Perugia, Italy
P. Asenov[a,56], G. M. Bilei[a], D. Ciangottini[a,b], L. Fanò[a,b], M. Magherini[a,b], G. Mantovani[a,b], V. Mariani[a,b], M. Menichelli[a], F. Moscatelli[a,56], A. Piccinelli[a,b], M. Presilla[a,b], A. Rossi[a,b], A. Santocchia[a,b], D. Spiga[a], T. Tedeschi[a,b]

INFN Sezione di Pisa[a], Università di Pisa[b], Scuola Normale Superiore di Pisa[c], Pisa, Italy; Università di Siena[d], Siena, Italy
P. Azzurri[a], G. Bagliesi[a], V. Bertacchi[a,c], R. Bhattacharya[a], L. Bianchini[a,b], T. Boccali[a], E. Bossini[a,b], D. Bruschini[a,c], R. Castaldi[a], M. A. Ciocci[a,b], V. D'Amante[a,d], R. Dell'Orso[a], M. R. Di Domenico[a,d], S. Donato[a], A. Giassi[a], F. Ligabue[a,c], G. Mandorli[a,c], D. Matos Figueiredo[a], A. Messineo[a,b], M. Musich[a,b], F. Palla[a], S. Parolia[a], G. Ramirez-Sanchez[a,c], A. Rizzi[a,b], G. Rolandi[a,c], S. Roy Chowdhury[a], T. Sarkar[a], A. Scribano[a], N. Shafiei[a,b], P. Spagnolo[a], R. Tenchini[a], G. Tonelli[a,b], N. Turini[a,d], A. Venturi[a], P. G. Verdini[a]

INFN Sezione di Roma[a], Sapienza Università di Roma[b], Rome, Italy
P. Barria[a], M. Campana[a,b], F. Cavallari[a], D. Del Re[a,b], E. Di Marco[a], M. Diemoz[a], E. Longo[a,b], P. Meridiani[a], G. Organtini[a,b], F. Pandolfi[a], R. Paramatti[a,b], C. Quaranta[a,b], S. Rahatlou[a,b], C. Rovelli[a], F. Santanastasio[a,b], L. Soffi[a], R. Tramontano[a,b]

INFN Sezione di Torino[a], Università di Torino[b], Torino, Italy; Università del Piemonte Orientale[c], Novara, Italy
N. Amapane[a,b], R. Arcidiacono[a,c], S. Argiro[a,b], M. Arneodo[a,c], N. Bartosik[a], R. Bellan[a,b], A. Bellora[a,b], C. Biino[a], N. Cartiglia[a], M. Costa[a,b], R. Covarelli[a,b], N. Demaria[a], M. Grippo[a,b], B. Kiani[a,b], F. Legger[a], C. Mariotti[a], S. Maselli[a], A. Mecca[a,b], E. Migliore[a,b], E. Monteil[a,b], M. Monteno[a], R. Mulargia[a], M. M. Obertino[a,b], G. Ortona[a], L. Pacher[a,b], N. Pastrone[a], M. Pelliccioni[a], M. Ruspa[a,c], K. Shchelina[a], F. Siviero[a,b], V. Sola[a,b], A. Solano[a,b], D. Soldi[a,b], A. Staiano[a], M. Tornago[a,b], D. Trocino[a], G. Umoret[a,b], A. Vagnerini[a,b]

INFN Sezione di Trieste[a], Università di Trieste[b], Trieste, Italy
S. Belforte[a], V. Candelise[a,b], M. Casarsa[a], F. Cossutti[a], A. Da Rold[a,b], G. Della Ricca[a,b], G. Sorrentino[a,b]

Kyungpook National University, Daegu, Korea
S. Dogra, C. Huh, B. Kim, D. H. Kim, G. N. Kim, J. Kim, J. Lee, S. W. Lee, C. S. Moon, Y. D. Oh, S. I. Pak, M. S. Ryu, S. Sekmen, Y. C. Yang

Chonnam National University, Institute for Universe and Elementary Particles, Kwangju, Korea
H. Kim, D. H. Moon

Hanyang University, Seoul, Korea
E. Asilar, T. J. Kim, J. Park

Korea University, Seoul, Korea
S. Choi, S. Han, B. Hong, K. Lee, K. S. Lee, J. Lim, J. Park, S. K. Park, J. Yoo

Department of Physics, Kyung Hee University, Seoul, Korea
J. Goh

Sejong University, Seoul, Korea
H. S. Kim, Y. Kim, S. Lee

Seoul National University, Seoul, Korea
J. Almond, J. H. Bhyun, J. Choi, S. Jeon, J. Kim, J. S. Kim, S. Ko, H. Kwon, H. Lee, S. Lee, B. H. Oh, S. B. Oh, H. Seo, U. K. Yang, I. Yoon

University of Seoul, Seoul, Korea
W. Jang, D. Y. Kang, Y. Kang, D. Kim, S. Kim, B. Ko, J. S. H. Lee, Y. Lee, J. A. Merlin, I. C. Park, Y. Roh, D. Song, I. J. Watson, S. Yang

Department of Physics, Yonsei University, Seoul, Korea
S. Ha, H. D. Yoo

Sungkyunkwan University, Suwon, Korea
M. Choi, M. R. Kim, H. Lee, Y. Lee, Y. Lee, I. Yu

College of Engineering and Technology, American University of the Middle East (AUM), Dasman, Kuwait
T. Beyrouthy, Y. Maghrbi

Riga Technical University, Riga, Latvia
K. Dreimanis, G. Pikurs, A. Potrebko, M. Seidel, V. Veckalns[57]

Vilnius University, Vilnius, Lithuania
M. Ambrozas, A. Carvalho Antunes De Oliveira, A. Juodagalvis, A. Rinkevicius, G. Tamulaitis

National Centre for Particle Physics, Universiti Malaya, Kuala Lumpur, Malaysia
N. Bin Norjoharuddeen, S. Y. Hoh[58], I. Yusuff[58], Z. Zolkapli

Universidad de Sonora (UNISON), Hermosillo, Mexico
J. F. Benitez, A. Castaneda Hernandez, H. A. Encinas Acosta, L. G. Gallegos Maríñez, M. León Coello, J. A. Murillo Quijada, A. Sehrawat, L. Valencia Palomo

Centro de Investigacion y de Estudios Avanzados del IPN, Mexico City, Mexico
G. Ayala, H. Castilla-Valdez, I. Heredia-De La Cruz[59], R. Lopez-Fernandez, C. A. Mondragon Herrera, D. A. Perez Navarro, A. Sánchez Hernández

Universidad Iberoamericana, Mexico City, Mexico
C. Oropeza Barrera, F. Vazquez Valencia

Benemerita Universidad Autonoma de Puebla, Puebla, Mexico
I. Pedraza, H. A. Salazar Ibarguen, C. Uribe Estrada

University of Montenegro, Podgorica, Montenegro
I. Bubanja, J. Mijuskovic[60], N. Raicevic

National Centre for Physics, Quaid-I-Azam University, Islamabad, Pakistan
A. Ahmad, M. I. Asghar, A. Awais, M. I. M. Awan, M. Gul, H. R. Hoorani, W. A. Khan, M. Shoaib, M. Waqas

AGH University of Science and Technology Faculty of Computer Science, Electronics and Telecommunications, Kraków, Poland
V. Avati, L. Grzanka, M. Malawski

National Centre for Nuclear Research, Swierk, Poland
H. Bialkowska, M. Bluj, B. Boimska, M. Górski, M. Kazana, M. Szleper, P. Zalewski

Institute of Experimental Physics, Faculty of Physics, University of Warsaw, Warsaw, Poland
K. Bunkowski, K. Doroba, A. Kalinowski, M. Konecki, J. Krolikowski

Laboratório de Instrumentação e Física Experimental de Partículas, Lisbon, Portugal
M. Araujo, P. Bargassa, D. Bastos, A. Boletti, P. Faccioli, M. Gallinaro, J. Hollar, N. Leonardo, T. Niknejad, M. Pisano, J. Seixas, J. Varela

VINCA Institute of Nuclear Sciences, University of Belgrade, Belgrade, Serbia
P. Adzic[61], M. Dordevic, P. Milenovic, J. Milosevic

Centro de Investigaciones Energéticas Medioambientales y Tecnológicas (CIEMAT), Madrid, Spain
M. Aguilar-Benitez, J. Alcaraz Maestre, A. Álvarez Fernández, M. Barrio Luna, Cristina F. Bedoya, C. A. Carrillo Montoya, M. Cepeda, M. Cerrada, N. Colino, M. Czakon[62], B. De La Cruz, A. Delgado Peris, D. Fernández Del Val, J. P. Fernández Ramos, J. Flix, M. C. Fouz, O. Gonzalez Lopez, S. Goy Lopez, J. M. Hernandez, M. I. Josa, J. León Holgado, A. Mitov[63], D. Moran, M. Pellen[64], C. Perez Dengra, A. Pérez-Calero Yzquierdo, R. Poncelet[63], J. Puerta Pelayo, I. Redondo, D. D. Redondo Ferrero, L. Romero, S. Sánchez Navas, J. Sastre, L. Urda Gómez, J. Vazquez Escobar, C. Willmott

Universidad Autónoma de Madrid, Madrid, Spain
J. F. de Trocóniz

Instituto Universitario de Ciencias y Tecnologías Espaciales de Asturias (ICTEA), Universidad de Oviedo, Oviedo, Spain
B. Alvarez Gonzalez, J. Cuevas, J. Fernandez Menendez, S. Folgueras, I. Gonzalez Caballero, J. R. González Fernández, E. Palencia Cortezon, C. Ramón Álvarez, V. Rodríguez Bouza, A. Soto Rodríguez, A. Trapote, C. Vico Villalba

Instituto de Física de Cantabria (IFCA), CSIC-Universidad de Cantabria, Santander, Spain
J. A. Brochero Cifuentes, I. J. Cabrillo, A. Calderon, J. Duarte Campderros, M. Fernandez, C. Fernandez Madrazo, A. García Alonso, G. Gomez, C. Lasaosa García, C. Martinez Rivero, P. Martinez Ruiz del Arbol, F. Matorras, P. Matorras Cuevas, J. Piedra Gomez, C. Prieels, L. Scodellaro, I. Vila, J. M. Vizan Garcia

University of Colombo, Colombo, Sri Lanka
M. K. Jayananda, B. Kailasapathy[65], D. U. J. Sonnadara, D. D. C. Wickramarathna

University of Ruhuna, Department of Physics, Matara, Sri Lanka
W. G. D. Dharmaratna, K. Liyanage, N. Perera, N. Wickramage

CERN, European Organization for Nuclear Research, Geneva, Switzerland
D. Abbaneo, J. Alimena, E. Auffray, G. Auzinger, J. Baechler, P. Baillon[†], D. Barney, J. Bendavid, M. Bianco, B. Bilin, A. Bocci, E. Brondolin, C. Caillol, T. Camporesi, G. Cerminara, N. Chernyavskaya, S. S. Chhibra, S. Choudhury, M. Cipriani, L. Cristella, D. d'Enterria, A. Dabrowski, A. David, A. De Roeck, M. M. Defranchis, M. Deile, M. Dobson, M. Dünser, N. Dupont, F. Fallavollita[66], A. Florent, L. Forthomme, G. Franzoni, W. Funk, S. Ghosh, S. Giani, D. Gigi, K. Gill, F. Glege, L. Gouskos, E. Govorkova, M. Haranko, J. Hegeman, V. Innocente, T. James, P. Janot, J. Kaspar, J. Kieseler, N. Kratochwil, S. Laurila, P. Lecoq, E. Leutgeb, C. Lourenço, B. Maier, L. Malgeri, M. Mannelli, A. C. Marini, F. Meijers, S. Mersi, E. Meschi, F. Moortgat, M. Mulders, S. Orfanelli, L. Orsini, F. Pantaleo, E. Perez, M. Peruzzi, A. Petrilli, G. Petrucciani, A. Pfeiffer, M. Pierini, D. Piparo, M. Pitt, H. Qu, T. Quast, D. Rabady, A. Racz, G. Reales Gutiérrez, M. Rovere, H. Sakulin, J. Salfeld-Nebgen, S. Scarfi, M. Selvaggi, A. Sharma, P. Silva, P. Sphicas[67], A. G. Stahl Leiton, S. Summers, K. Tatar, V. R. Tavolaro, D. Treille, P. Tropea, A. Tsirou, J. Wanczyk[68], K. A. Wozniak, W. D. Zeuner

Paul Scherrer Institut, Villigen, Switzerland
L. Caminada[69], A. Ebrahimi, W. Erdmann, R. Horisberger, Q. Ingram, H. C. Kaestli, D. Kotlinski, C. Lange, M. Missiroli[69], L. Noehte[69], T. Rohe

ETH Zurich-Institute for Particle Physics and Astrophysics (IPA), Zurich, Switzerland
T. K. Aarrestad, K. Androsov[68], M. Backhaus, P. Berger, A. Calandri, K. Datta, A. De Cosa, G. Dissertori, M. Dittmar, M. Donegà, F. Eble, M. Galli, K. Gedia, F. Glessgen, T. A. Gómez Espinosa, C. Grab, D. Hits, W. Lustermann, A.-M. Lyon, R. A. Manzoni, L. Marchese, C. Martin Perez, A. Mascellani[68], F. Nessi-Tedaldi, J. Niedziela, F. Pauss, V. Perovic, S. Pigazzini, M. G. Ratti, M. Reichmann, C. Reissel, T. Reitenspiess, B. Ristic, F. Riti, D. Ruini, D. A. Sanz Becerra, J. Steggemann[68], D. Valsecchi[27], R. Wallny

Universität Zürich, Zurich, Switzerland
C. Amsler[70], P. Bärtschi, C. Botta, D. Brzhechko, M. F. Canelli, K. Cormier, A. De Wit, R. Del Burgo, J. K. Heikkilä, M. Huwiler, W. Jin, A. Jofrehei, B. Kilminster, S. Leontsinis, S. P. Liechti, A. Macchiolo, P. Meiring, V. M. Mikuni, U. Molinatti, I. Neutelings, A. Reimers, P. Robmann, S. Sanchez Cruz, K. Schweiger, M. Senger, Y. Takahashi

National Central University, Chung-Li, Taiwan
C. Adloff[71], C. M. Kuo, W. Lin, P. K. Rout, S. S. Yu

National Taiwan University (NTU), Taipei, Taiwan
L. Ceard, Y. Chao, K. F. Chen, P.s. Chen, H. Cheng, W.-S. Hou, R. Khurana, G. Kole, Y.y. Li, R.-S. Lu, E. Paganis, A. Psallidas, A. Steen, H.y. Wu, E. Yazgan, P.r. Yu

Department of Physics, Faculty of Science, Chulalongkorn University, Bangkok, Thailand
C. Asawatangtrakuldee, N. Srimanobhas, V. Wachirapusitanand

Physics Department, Science and Art Faculty, Çukurova University, Adana, Turkey
D. Agyel, F. Boran, Z. S. Demiroglu, F. Dolek, I. Dumanoglu[72], E. Eskut, Y. Guler[73], E. Gurpinar Guler[73], C. Isik, O. Kara, A. Kayis Topaksu, U. Kiminsu, G. Onengut, K. Ozdemir[74], A. Polatoz, A. E. Simsek, B. Tali[75], U. G. Tok, S. Turkcapar, E. Uslan, I. S. Zorbakir

Physics Department, Middle East Technical University, Ankara, Turkey
G. Karapinar[76], K. Ocalan[77], M. Yalvac[78]

Bogazici University, Istanbul, Turkey
B. Akgun, I. O. Atakisi, E. Gülmez, M. Kaya[79], O. Kaya[80], S. Tekten[81]

Istanbul Technical University, Istanbul, Turkey
A. Cakir, K. Cankocak[72], Y. Komurcu, S. Sen[72]

Istanbul University, Istanbul, Turkey
O. Aydilek, S. Cerci[75], B. Hacisahinoglu, I. Hos[82], B. Isildak[83], B. Kaynak, S. Ozkorucuklu, C. Simsek, D. Sunar Cerci[75]

Institute for Scintillation Materials of National Academy of Science of Ukraine, Kharkiv, Ukraine
B. Grynyov

National Science Centre, Kharkiv Institute of Physics and Technology, Kharkiv, Ukraine
L. Levchuk

University of Bristol, Bristol, UK
D. Anthony, E. Bhal, J. J. Brooke, A. Bundock, E. Clement, D. Cussans, H. Flacher, M. Glowacki, J. Goldstein, H. F. Heath, L. Kreczko, B. Krikler, S. Paramesvaran, S. Seif El Nasr-Storey, V. J. Smith, N. Stylianou[84], K. Walkingshaw Pass, R. White

Rutherford Appleton Laboratory, Didcot, UK
A. H. Ball, K. W. Bell, A. Belyaev[85], C. Brew, R. M. Brown, D. J. A. Cockerill, C. Cooke, K. V. Ellis,

K. Harder, S. Harper, M.-L. Holmberg[86], Sh. Jain, J. Linacre, K. Manolopoulos, D. M. Newbold, E. Olaiya, D. Petyt, T. Reis, G. Salvi, T. Schuh, C. H. Shepherd-Themistocleous, I. R. Tomalin, T. Williams

Imperial College, London, UK
R. Bainbridge, P. Bloch, S. Bonomally, J. Borg, C. E. Brown, O. Buchmuller, V. Cacchio, V. Cepaitis, G. S. Chahal[87], D. Colling, J. S. Dancu, P. Dauncey, G. Davies, J. Davies, M. Della Negra, S. Fayer, G. Fedi, G. Hall, M. H. Hassanshahi, A. Howard, G. Iles, J. Langford, L. Lyons, A.-M. Magnan, S. Malik, A. Martelli, M. Mieskolainen, D. G. Monk, J. Nash[88], M. Pesaresi, B. C. Radburn-Smith, D. M. Raymond, A. Richards, A. Rose, E. Scott, C. Seez, R. Shukla, A. Tapper, K. Uchida, G. P. Uttley, L. H. Vage, T. Virdee[27], M. Vojinovic, N. Wardle, S. N. Webb, D. Winterbottom

Brunel University, Uxbridge, UK
K. Coldham, J. E. Cole, A. Khan, P. Kyberd, I. D. Reid

Baylor University, Waco, TX, USA
S. Abdullin, A. Brinkerhoff, B. Caraway, J. Dittmann, K. Hatakeyama, A. R. Kanuganti, B. McMaster, M. Saunders, S. Sawant, C. Sutantawibul, M. Toms, J. Wilson

Catholic University of America, Washington, DC, USA
R. Bartek, A. Dominguez, R. Uniyal, A. M. Vargas Hernandez

The University of Alabama, Tuscaloosa, AL, USA
S. I. Cooper, D. Di Croce, S. V. Gleyzer, C. Henderson, C. U. Perez, P. Rumerio[89], C. West

Boston University, Boston, MA, USA
A. Akpinar, A. Albert, D. Arcaro, C. Cosby, Z. Demiragli, C. Erice, E. Fontanesi, D. Gastler, S. May, J. Rohlf, K. Salyer, D. Sperka, D. Spitzbart, I. Suarez, A. Tsatsos, S. Yuan

Brown University, Providence, RI, USA
G. Benelli, B. Burkle, X. Coubez[22], D. Cutts, M. Hadley, U. Heintz, J. M. Hogan[90], T. Kwon, G. Landsberg, K. T. Lau, D. Li, J. Luo, M. Narain, N. Pervan, S. Sagir[91], F. Simpson, E. Usai, W. Y. Wong, X. Yan, D. Yu, W. Zhang

University of California, Davis, Davis, CA, USA
J. Bonilla, C. Brainerd, R. Breedon, M. Calderon De La Barca Sanchez, M. Chertok, J. Conway, P. T. Cox, R. Erbacher, G. Haza, F. Jensen, O. Kukral, G. Mocellin, M. Mulhearn, D. Pellett, B. Regnery, Y. Yao, F. Zhang

University of California, Los Angeles, CA, USA
M. Bachtis, R. Cousins, A. Datta, D. Hamilton, J. Hauser, M. Ignatenko, M. A. Iqbal, T. Lam, E. Manca, W. A. Nash, S. Regnard, D. Saltzberg, B. Stone, V. Valuev

University of California, Riverside, Riverside, CA, USA
R. Clare, J. W. Gary, M. Gordon, G. Hanson, G. Karapostoli, O. R. Long, N. Manganelli, W. Si, S. Wimpenny

University of California, San Diego, La Jolla, CA, USA
J. G. Branson, P. Chang, S. Cittolin, S. Cooperstein, D. Diaz, J. Duarte, R. Gerosa, L. Giannini, J. Guiang, R. Kansal, V. Krutelyov, R. Lee, J. Letts, M. Masciovecchio, F. Mokhtar, M. Pieri, B. V. Sathia Narayanan, V. Sharma, M. Tadel, E. Vourliotis, F. Würthwein, Y. Xiang, A. Yagil

Department of Physics, University of California, Santa Barbara, Santa Barbara, CA, USA
N. Amin, C. Campagnari, M. Citron, G. Collura, A. Dorsett, V. Dutta, J. Incandela, M. Kilpatrick, J. Kim, A. J. Li, P. Masterson, H. Mei, M. Oshiro, M. Quinnan, J. Richman, U. Sarica, R. Schmitz, F. Setti, J. Sheplock, P. Siddireddy, D. Stuart, S. Wang

California Institute of Technology, Pasadena, CA, USA
A. Bornheim, O. Cerri, I. Dutta, A. Latorre, J. M. Lawhorn, J. Mao, H. B. Newman, T. Q. Nguyen, M. Spiropulu, J. R. Vlimant, C. Wang, S. Xie, R. Y. Zhu

Carnegie Mellon University, Pittsburgh, PA, USA
J. Alison, S. An, M. B. Andrews, P. Bryant, T. Ferguson, A. Harilal, C. Liu, T. Mudholkar, S. Murthy, M. Paulini, A. Roberts, A. Sanchez, W. Terrill

University of Colorado Boulder, Boulder, CO, USA
J. P. Cumalat, W. T. Ford, A. Hassani, G. Karathanasis, E. MacDonald, F. Marini, A. Perloff, C. Savard, N. Schonbeck, K. Stenson, K. A. Ulmer, S. R. Wagner, N. Zipper

Cornell University, Ithaca, NY, USA
J. Alexander, S. Bright-Thonney, X. Chen, D. J. Cranshaw, J. Fan, X. Fan, D. Gadkari, S. Hogan, J. Monroy, J. R. Patterson, D. Quach, J. Reichert, M. Reid, A. Ryd, J. Thom, P. Wittich, R. Zou

Fermi National Accelerator Laboratory, Batavia, IL, USA
M. Albrow, M. Alyari, G. Apollinari, A. Apresyan, L. A. T. Bauerdick, D. Berry, J. Berryhill, P. C. Bhat, K. Burkett, J. N. Butler, A. Canepa, G. B. Cerati, H. W. K. Cheung, F. Chlebana, K. F. Di Petrillo, J. Dickinson, V. D. Elvira, Y. Feng, J. Freeman, A. Gandrakota, Z. Gecse, L. Gray, D. Green, S. Grünendahl, D. Guerrero, O. Gutsche, R. M. Harris, R. Heller, T. C. Herwig, J. Hirschauer, L. Horyn, B. Jayatilaka, S. Jindariani, M. Johnson, U. Joshi, T. Klijnsma, B. Klima, K. H. M. Kwok, S. Lammel, D. Lincoln, R. Lipton, T. Liu, C. Madrid, K. Maeshima, C. Mantilla, D. Mason, P. McBride, P. Merkel, S. Mrenna, S. Nahn, J. Ngadiuba, D. Noonan, V. Papadimitriou, N. Pastika, K. Pedro, C. Pena[92], F. Ravera, A. Reinsvold Hall[93], L. Ristori, E. Sexton-Kennedy, N. Smith, A. Soha, L. Spiegel, J. Strait, L. Taylor, S. Tkaczyk, N. V. Tran, L. Uplegger, E. W. Vaandering, I. Zoi

University of Florida, Gainesville, FL, USA
P. Avery, D. Bourilkov, L. Cadamuro, V. Cherepanov, R. D. Field, M. Kim, E. Koenig, J. Konigsberg, A. Korytov, E. Kuznetsova[94], K. H. Lo, K. Matchev, N. Menendez, G. Mitselmakher, A. Muthirakalayil Madhu, N. Rawal, D. Rosenzweig, S. Rosenzweig, K. Shi, J. Wang, Z. Wu

Florida State University, Tallahassee, FL, USA
T. Adams, A. Askew, N. Bower, R. Habibullah, V. Hagopian, T. Kolberg, G. Martinez, H. Prosper, O. Viazlo, M. Wulansatiti, R. Yohay, J. Zhang

Florida Institute of Technology, Melbourne, FL, USA
M. M. Baarmand, S. Butalla, T. Elkafrawy[55], M. Hohlmann, R. Kumar Verma, M. Rahmani, F. Yumiceva

University of Illinois at Chicago (UIC), Chicago, IL, USA
M. R. Adams, H. Becerril Gonzalez, R. Cavanaugh, S. Dittmer, O. Evdokimov, C. E. Gerber, D. J. Hofman, D. S. Lemos, A. H. Merrit, C. Mills, G. Oh, T. Roy, S. Rudrabhatla, M. B. Tonjes, N. Varelas, X. Wang, Z. Ye, J. Yoo

The University of Iowa, Iowa City, IA, USA
M. Alhusseini, K. Dilsiz[95], L. Emediato, G. Karaman, O. K. Köseyan, J.-P. Merlo, A. Mestvirishvili[96], J. Nachtman, O. Neogi, H. Ogul[97], Y. Onel, A. Penzo, C. Snyder, E. Tiras[98]

Johns Hopkins University, Baltimore, MD, USA
O. Amram, B. Blumenfeld, L. Corcodilos, J. Davis, A. V. Gritsan, S. Kyriacou, P. Maksimovic, J. Roskes, S. Sekhar, M. Swartz, T.Á. Vámi

The University of Kansas, Lawrence, KS, USA
A. Abreu, L. F. Alcerro Alcerro, J. Anguiano, P. Baringer, A. Bean, Z. Flowers, T. Isidori, J. King, G. Krintiras, M. Lazarovits, C. Le Mahieu, C. Lindsey, J. Marquez, N. Minafra, M. Murray, M. Nickel, C. Rogan, C. Royon, R. Salvatico, S. Sanders, C. Smith, Q. Wang, G. Wilson

Kansas State University, Manhattan, KS, USA
B. Allmond, S. Duric, A. Ivanov, K. Kaadze, A. Kalogeropoulos, D. Kim, Y. Maravin, T. Mitchell, A. Modak, K. Nam, D. Roy

Lawrence Livermore National Laboratory, Livermore, CA, USA
F. Rebassoo, D. Wright

University of Maryland, College Park, MD, USA
E. Adams, A. Baden, O. Baron, A. Belloni, A. Bethani, S. C. Eno, N. J. Hadley, S. Jabeen, R. G. Kellogg, T. Koeth, Y. Lai, S. Lascio, A. C. Mignerey, S. Nabili, C. Palmer, C. Papageorgakis, L. Wang, K. Wong

Massachusetts Institute of Technology, Cambridge, MA, USA
D. Abercrombie, W. Busza, I. A. Cali, Y. Chen, M. D'Alfonso, J. Eysermans, C. Freer, G. Gomez-Ceballos, M. Goncharov, P. Harris, M. Hu, D. Kovalskyi, J. Krupa, Y.-J. Lee, K. Long, C. Mironov, C. Paus, D. Rankin, C. Roland, G. Roland, Z. Shi, G. S. F. Stephans, J. Wang, Z. Wang, B. Wyslouch, T. J. Yang

University of Minnesota, Minneapolis, MN, USA
R. M. Chatterjee, B. Crossman, A. Evans, J. Hiltbrand, B. M. Joshi, C. Kapsiak, M. Krohn, Y. Kubota, J. Mans, M. Revering, R. Rusack, R. Saradhy, N. Schroeder, N. Strobbe, M. A. Wadud

University of Mississippi, Oxford, MS, USA
L. M. Cremaldi

University of Nebraska-Lincoln, Lincoln, NE, USA
K. Bloom, M. Bryson, D. R. Claes, C. Fangmeier, L. Finco, F. Golf, C. Joo, R. Kamalieddin, I. Kravchenko, I. Reed, J. E. Siado, G. R. Snow†, W. Tabb, A. Wightman, F. Yan, A. G. Zecchinelli

State University of New York at Buffalo, Buffalo, NY, USA
G. Agarwal, H. Bandyopadhyay, L. Hay, I. Iashvili, A. Kharchilava, C. McLean, M. Morris, D. Nguyen, J. Pekkanen, S. Rappoccio, A. Williams

Northeastern University, Boston, MA, USA
G. Alverson, E. Barberis, Y. Haddad, Y. Han, A. Krishna, J. Li, J. Lidrych, G. Madigan, B. Marzocchi, D. M. Morse, V. Nguyen, T. Orimoto, A. Parker, L. Skinnari, A. Tishelman-Charny, T. Wamorkar, B. Wang, A. Wisecarver, D. Wood

Northwestern University, Evanston, IL, USA
S. Bhattacharya, J. Bueghly, Z. Chen, A. Gilbert, K. A. Hahn, Y. Liu, N. Odell, M. H. Schmitt, M. Velasco

University of Notre Dame, Notre Dame, IN, USA
R. Band, R. Bucci, M. Cremonesi, A. Das, R. Goldouzian, M. Hildreth, K. Hurtado Anampa, C. Jessop, K. Lannon, J. Lawrence, N. Loukas, L. Lutton, J. Mariano, N. Marinelli, I. Mcalister, T. McCauley, C. Mcgrady, K. Mohrman, C. Moore, Y. Musienko[12], R. Ruchti, A. Townsend, M. Wayne, H. Yockey, M. Zarucki, L. Zygala

The Ohio State University, Columbus, OH, USA
B. Bylsma, M. Carrigan, L. S. Durkin, B. Francis, C. Hill, M. Joyce, A. Lesauvage, M. Nunez Ornelas, K. Wei, B. L. Winer, B. R. Yates

Princeton University, Princeton, NJ, USA
F. M. Addesa, P. Das, G. Dezoort, P. Elmer, A. Frankenthal, B. Greenberg, N. Haubrich, S. Higginbotham, G. Kopp, S. Kwan, D. Lange, D. Marlow, I. Ojalvo, J. Olsen, D. Stickland, C. Tully

University of Puerto Rico, Mayaguez, PR, USA
S. Malik, S. Norberg

Purdue University, West Lafayette, IN, USA
A. S. Bakshi, V. E. Barnes, R. Chawla, S. Das, L. Gutay, M. Jones, A. W. Jung, D. Kondratyev, A. M. Koshy, M. Liu, G. Negro, N. Neumeister, G. Paspalaki, S. Piperov, A. Purohit, J. F. Schulte, M. Stojanovic[15], J. Thieman, F. Wang, R. Xiao, W. Xie

Purdue University Northwest, Hammond, IN, USA
J. Dolen, N. Parashar

Rice University, Houston, TX, USA
D. Acosta, A. Baty, T. Carnahan, S. Dildick, K. M. Ecklund, P. J. Fernández Manteca, S. Freed, P. Gardner, F. J. M. Geurts, A. Kumar, W. Li, B. P. Padley, R. Redjimi, J. Rotter, S. Yang, E. Yigitbasi, L. Zhang[99], Y. Zhang

University of Rochester, Rochester, NY, USA
A. Bodek, P. de Barbaro, R. Demina, J. L. Dulemba, C. Fallon, T. Ferbel, M. Galanti, A. Garcia-Bellido, O. Hindrichs, A. Khukhunaishvili, P. Parygin, E. Popova, E. Ranken, R. Taus, G. P. Van Onsem

The Rockefeller University, New York, NY, USA
K. Goulianos

Rutgers, The State University of New Jersey, Piscataway, NJ, USA
B. Chiarito, J. P. Chou, Y. Gershtein, E. Halkiadakis, A. Hart, M. Heindl, D. Jaroslawski, O. Karacheban[25], I. Laflotte, A. Lath, R. Montalvo, K. Nash, M. Osherson, H. Routray, S. Salur, S. Schnetzer, S. Somalwar, R. Stone, S. A. Thayil, S. Thomas, H. Wang

University of Tennessee, Knoxville, TN, USA
H. Acharya, A. G. Delannoy, S. Fiorendi, T. Holmes, E. Nibigira, S. Spanier

Texas A&M University, College Station, TX, USA
O. Bouhali[100], M. Dalchenko, A. Delgado, R. Eusebi, J. Gilmore, T. Huang, T. Kamon[101], H. Kim, S. Luo, S. Malhotra, R. Mueller, D. Overton, D. Rathjens, A. Safonov

Texas Tech University, Lubbock, TX, USA
N. Akchurin, J. Damgov, V. Hegde, K. Lamichhane, S. W. Lee, T. Mengke, S. Muthumuni, T. Peltola, I. Volobouev, A. Whitbeck

Vanderbilt University, Nashville, TN, USA
E. Appelt, S. Greene, A. Gurrola, W. Johns, A. Melo, F. Romeo, P. Sheldon, S. Tuo, J. Velkovska, J. Viinikainen

University of Virginia, Charlottesville, VA, USA
B. Cardwell, B. Cox, G. Cummings, J. Hakala, R. Hirosky, A. Ledovskoy, A. Li, C. Neu, C. E. Perez Lara, B. Tannenwald

Wayne State University, Detroit, MI, USA
P. E. Karchin, N. Poudyal

University of Wisconsin-Madison, Madison, WI, USA
S. Banerjee, K. Black, T. Bose, S. Dasu, I. De Bruyn, P. Everaerts, C. Galloni, H. He, M. Herndon, A. Herve, C. K. Koraka, A. Lanaro, A. Loeliger, R. Loveless, J. Madhusudanan Sreekala, A. Mallampalli, A. Mohammadi, S. Mondal, G. Parida, D. Pinna, A. Savin, V. Shang, V. Sharma, W. H. Smith, D. Teague, H. F. Tsoi, W. Vetens

Authors affiliated with an institute or an international laboratory covered by a cooperation agreement with CERN, Geneva, Switzerland
S. Afanasiev, V. Andreev, Yu. Andreev, T. Aushev, M. Azarkin, A. Babaev, A. Belyaev, V. Blinov[102], E. Boos, V. Borshch, D. Budkouski, V. Chekhovsky, R. Chistov[102], M. Danilov[102], A. Dermenev, T. Dimova[102], I. Dremin, M. Dubinin[92], L. Dudko, V. Epshteyn, A. Ershov, G. Gavrilov, V. Gavrilov, S. Gninenko, V. Golovtcov, N. Golubev, I. Golutvin, I. Gorbunov, A. Gribushin, Y. Ivanov, V. Kachanov, L. Kardapoltsev[102], V. Karjavine, A. Karneyeu, V. Kim[102], M. Kirakosyan, D. Kirpichnikov, M. Kirsanov, V. Klyukhin, O. Kodolova[103], D. Konstantinov, V. Korenkov, A. Kozyrev[102], N. Krasnikov, A. Lanev, P. Levchenko, A. Litomin, N. Lychkovskaya, V. Makarenko, A. Malakhov, V. Matveev[102], V. Murzin, A. Nikitenko[104], S. Obraztsov, A. Oskin, I. Ovtin[102], V. Palichik, V. Perelygin, S. Petrushanko, S. Polikarpov[102], V. Popov, O. Radchenko[102], M. Savina, V. Savrin, V. Shalaev, S. Shmatov, S. Shulha, Y. Skovpen[102], S. Slabospitskii, V. Smirnov, A. Snigirev, D. Sosnov,

V. Sulimov, E. Tcherniaev, A. Terkulov, O. Teryaev, I. Tlisova, A. Toropin, L. Uvarov, A. Uzunian, E. Vlasov, A. Vorobyev, N. Voytishin, B. S. Yuldashev[105], A. Zarubin, I. Zhizhin, A. Zhokin

† **Deceased**

1: Also at Yerevan State University, Yerevan, Armenia
2: Also at TU Wien, Vienna, Austria
3: Also at Institute of Basic and Applied Sciences, Faculty of Engineering, Arab Academy for Science, Technology and Maritime Transport, Alexandria, Egypt
4: Also at Université Libre de Bruxelles, Bruxelles, Belgium
5: Also at Universidade Estadual de Campinas, Campinas, Brazil
6: Also at Federal University of Rio Grande do Sul, Porto Alegre, Brazil
7: Also at UFMS, Nova Andradina, Brazil
8: Also at University of Chinese Academy of Sciences, Beijing, China
9: Also at Nanjing Normal University, Nanjing, China
10: Now at The University of Iowa, Iowa City, IA, USA
11: Also at University of Chinese Academy of Sciences, Beijing, China
12: Also at An institute or an international laboratory covered by a cooperation agreement with CERN, Geneva, Switzerland
13: Now at British University in Egypt, Cairo, Egypt
14: Now at Cairo University, Cairo, Egypt
15: Also at Purdue University, West Lafayette, IN, USA
16: Also at Université de Haute Alsace, Mulhouse, France
17: Also at Department of Physics, Tsinghua University, Beijing, China
18: Also at Ilia State University, Tbilisi, Georgia
19: Also at The University of the State of Amazonas, Manaus, Brazil
20: Also at Erzincan Binali Yildirim University, Erzincan, Turkey
21: Also at University of Hamburg, Hamburg, Germany
22: Also at III. Physikalisches Institut A, RWTH Aachen University, Aachen, Germany
23: Also at Isfahan University of Technology, Isfahan, Iran
24: Also at Bergische University Wuppertal (BUW), Wuppertal, Germany
25: Also at Brandenburg University of Technology, Cottbus, Germany
26: Also at Forschungszentrum Jülich, Juelich, Germany
27: Also at CERN, European Organization for Nuclear Research, Geneva, Switzerland
28: Also at Physics Department, Faculty of Science, Assiut University, Assiut, Egypt
29: Also at Karoly Robert Campus, MATE Institute of Technology, Gyongyos, Hungary
30: Also at Wigner Research Centre for Physics, Budapest, Hungary
31: Also at Institute of Physics, University of Debrecen, Debrecen, Hungary
32: Also at Institute of Nuclear Research ATOMKI, Debrecen, Hungary
33: Now at Universitatea Babes-Bolyai-Facultatea de Fizica, Cluj-Napoca, Romania
34: Also at Faculty of Informatics, University of Debrecen, Debrecen, Hungary
35: Also at Punjab Agricultural University, Ludhiana, India
36: Also at UPES-University of Petroleum and Energy Studies, Dehradun, India
37: Also at University of Visva-Bharati, Santiniketan, India
38: Also at University of Hyderabad, Hyderabad, India
39: Also at Indian Institute of Science (IISc), Bangalore, India
40: Also at Indian Institute of Technology (IIT), Mumbai, India
41: Also at IIT Bhubaneswar, Bhubaneswar, India
42: Also at Institute of Physics, Bhubaneswar, India
43: Also at Deutsches Elektronen-Synchrotron, Hamburg, Germany
44: Now at Department of Physics, Isfahan University of Technology, Isfahan, Iran
45: Also at Sharif University of Technology, Tehran, Iran
46: Also at Department of Physics, University of Science and Technology of Mazandaran, Behshahr, Iran
47: Also at Helwan University, Cairo, Egypt
48: Also at Italian National Agency for New Technologies, Energy and Sustainable Economic Development, Bologna, Italy

49: Also at Centro Siciliano di Fisica Nucleare e di Struttura Della Materia, Catania, Italy
50: Also at Università degli Studi Guglielmo Marconi, Rome, Italy
51: Also at Scuola Superiore Meridionale, Università di Napoli 'Federico II', Naples, Italy
52: Also at Fermi National Accelerator Laboratory, Batavia, IL, USA
53: Also at Laboratori Nazionali di Legnaro dell'INFN, Legnaro, Italy
54: Also at Università di Napoli 'Federico II', Naples, Italy
55: Also at Ain Shams University, Cairo, Egypt
56: Also at Consiglio Nazionale delle Ricerche-Istituto Officina dei Materiali, Perugia, Italy
57: Also at Riga Technical University, Riga, Latvia
58: Also at Department of Applied Physics, Faculty of Science and Technology, Universiti Kebangsaan Malaysia, Bangi, Malaysia
59: Also at Consejo Nacional de Ciencia y Tecnología, Mexico City, Mexico
60: Also at IRFU, CEA, Université Paris-Saclay, Gif-sur-Yvette, France
61: Also at Faculty of Physics, University of Belgrade, Belgrade, Serbia
62: Also at Institut für Theoretische Teilchenphysik und Kosmologie, RWTH Aachen University, Aachen, Germany
63: Also at Cavendish Laboratory, University of Cambridge, Cambridge, UK
64: Also at Albert-Ludwigs-Universität Freiburg, Physikalisches Institut, Freiburg, Germany
65: Also at Trincomalee Campus, Eastern University, Sri Lanka, Nilaveli, Sri Lanka
66: Also at INFN Sezione di Pavia, Università di Pavia, Pavia, Italy
67: Also at National and Kapodistrian University of Athens, Athens, Greece
68: Also at Ecole Polytechnique Fédérale Lausanne, Lausanne, Switzerland
69: Also at Universität Zürich, Zurich, Switzerland
70: Also at Stefan Meyer Institute for Subatomic Physics, Vienna, Austria
71: Also at Laboratoire d'Annecy-le-Vieux de Physique des Particules, IN2P3-CNRS, Annecy-le-Vieux, France
72: Also at Near East University, Research Center of Experimental Health Science, Mersin, Turkey
73: Also at Konya Technical University, Konya, Turkey
74: Also at Izmir Bakircay University, Izmir, Turkey
75: Also at Adiyaman University, Adiyaman, Turkey
76: Also at Istanbul Gedik University, Istanbul, Turkey
77: Also at Necmettin Erbakan University, Konya, Turkey
78: Also at Bozok Universitetesi Rektörlügü, Yozgat, Turkey
79: Also at Marmara University, Istanbul, Turkey
80: Also at Milli Savunma University, Istanbul, Turkey
81: Also at Kafkas University, Kars, Turkey
82: Also at Faculty of Engineering, Istanbul University-Cerrahpasa, Istanbul, Turkey
83: Also at Yildiz Technical University, Istanbul, Turkey
84: Also at Vrije Universiteit Brussel, Brussel, Belgium
85: Also at School of Physics and Astronomy, University of Southampton, Southampton, UK
86: Also at University of Bristol, Bristol, UK
87: Also at IPPP Durham University, Durham, UK
88: Also at Faculty of Science, Monash University, Clayton, Australia
89: Also at Università di Torino, Turin, Italy
90: Also at Bethel University, St. Paul, MN, USA
91: Also at Karamanoğlu Mehmetbey University, Karaman, Turkey
92: Also at California Institute of Technology, Pasadena, CA, USA
93: Also at United States Naval Academy, Annapolis, MD, USA
94: Also at University of Florida, Gainesville, FL, USA
95: Also at Bingol University, Bingol, Turkey
96: Also at Georgian Technical University, Tbilisi, Georgia
97: Also at Sinop University, Sinop, Turkey
98: Also at Erciyes University, Kayseri, Turkey
99: Also at Institute of Modern Physics and Key Laboratory of Nuclear Physics and Ion-beam Application (MOE)-Fudan University, Shanghai, China

100: Also at Texas A&M University at Qatar, Doha, Qatar
101: Also at Kyungpook National University, Daegu, Korea
102: Also at another institute or international laboratory covered by a cooperation agreement with CERN, Geneva, Switzerland
103: Also at Yerevan Physics Institute, Yerevan, Armenia
104: Also at Imperial College, London, UK
105: Also at Institute of Nuclear Physics of the Uzbekistan Academy of Sciences, Tashkent, Uzbekistan